STXBP5/tomosyn regulates both the small Rho GTPase and the surface expression of AMPA receptors to control the dendritic stability of neurons

Abbreviated title: Tomosyn regulates dendritic stability of neurons

Wenjuan Shen, Michaela B.C. Kilander, Morgan S. Bridi, Jeannine A. Frei, Robert F. Niescier, Shiyong Huang, and Yu-Chih Lin*

Program in Neuroscience, Hussman Institute for Autism, Baltimore, MD 21201

*Correspondence: yclin@hussmanautism.org

Number of pages: 46

Number of figures: 8

Number of tables: 0

Number of words for abstract: 233

Number of words for introduction: 650

Number of words for discussion: 1416

Acknowledgements

This work is supported by Hussman Foundation grant HIAS15003 to Y-C. L, and HIAS18001 to SH. We want to thank Drs. Louis DeTolla and Turhan Coksaygan at the University of Maryland School of Medicine for providing veterinary service and consultation. The authors gratefully acknowledge Elizabeth Benevides and Drs. Gene J. Blatt and John P. Hussman for their edits and helpful comments on the manuscript.

Conflict of Interest: The authors declare no competing financial interests.

Abstract

Tomosyn, a protein encoded by syntaxin-1-binding protein 5 (*STXBP5*) gene, regulates neurotransmitter release, synaptic transmission, and partitioning of synaptic vesicle pools. However, the role of tomosyn in dendritic arborization, spine stability, and trafficking of ionotropic glutamate receptors remains to be elucidated. In this study, we have shown that knockdown of tomosyn in mouse primary neurons leads to an increase of RhoA GTPase activity accompanied by compromised dendritic arborization and loss of dendritic spines. Inhibiting RhoA signaling was sufficient to rescue the abnormal dendritic morphology. Tomosyn knockdown neurons also exhibited reduced miniature excitatory postsynaptic current (mEPSC) frequency. Additionally, aberrant surface expression of AMPA receptors was observed in tomosyn-deficient neurons. These findings suggest that tomosyn regulates dendritic stability through two mechanisms: 1) tomosyn functions as a RhoA inhibitor for the maintenance of dendritic arborization and dendritic spine stability; 2) tomosyn acts as a component of dendritic soluble *N*-ethylmaleimide-sensitive factor attachment protein receptor (SNARE) accessory proteins to regulate trafficking of glutamate receptors. Recent studies have shown that deletion and mutations of *STXBP5* are associated with autism spectrum disorder (ASD). Neurons expressing two autism-associated tomosyn variants, L412V or Y502C, were further examined and displayed loss-of-function phenotypes, including reduced dendritic complexity and spine density as well as decreased surface expression of AMPA receptors. This study uncovers a novel role of tomosyn in maintaining neuronal function, and also a potential pathway to explain the cellular pathology underlying tomosyn-associated ASD.

Significance Statement

Tomosyn, known as syntaxin-1-binding protein 5 (STXBP5), has been shown to regulate neurotransmission, and its deletion and mutations are linked to autism. Here, we investigated tomosyn's role in both the maintenance of neuronal morphology and the surface expression of glutamate receptors. We found that tomosyn functions as a novel RhoA inhibitor to promote neuronal stability, and interacts with dendritic SNARE machinery including syntaxin-4 to affect surface expression of AMPA receptors. We also elucidated two autism-associated tomosyn variants, L412V and Y502C, as loss-of-function mutations. These data suggest a novel pathway mediated by tomosyn to regulate neuronal stability and receptor trafficking. The two variants of tomosyn resulting in defects of these mechanisms may contribute to the cellular phenotypes observed in autism.

Introduction

Excitatory neurons are major projecting cells in the brain and extend complex dendritic arbors to establish extensive connections with other neurons. Mature neurons have actin-rich spines that protrude from dendrites, and are the major structures harboring excitatory postsynaptic components. Ionotropic glutamate receptors, including AMPA and NMDA receptors, cluster primarily on dendritic spines, and are responsible for basal excitatory synaptic transmission and synaptic plasticity (Lau and Zukin, 2007; Diering and Huganir, 2018; Reiner and Levitz, 2018). The precise regulation of the recycling and trafficking of glutamate receptors is critical for maintaining synaptic function. Cytoskeleton rearrangement by Rho-signaling pathways is another driving force that regulates neuronal stability and synaptic plasticity (Nakayama et al., 2000; Govek et al., 2004; Lin and Koleske, 2010). Evidence also suggests that dendritic SNARE proteins, such as syntaxin-4, SNAP-23 and SNAP-25, are involved in glutamate receptor trafficking by mediating membrane fusion at postsynaptic areas (Lau et al., 2010; Bin et al., 2018). Identifying molecules that regulate glutamate receptor trafficking and dendritic stability will allow us to better understand the underlying mechanisms that promote neuronal stability and function.

Tomosyn was first identified as a protein encoded by syntaxin-1-binding protein 5 (STXBP5) in rats (Fujita et al., 1998). Structurally, tomosyn contains an N-terminal WD40-repeat domain and a C-terminal coiled-coil motif (Masuda et al., 1998). The R-SNARE-like structure at the C-terminus allows tomosyn to inhibit the formation of the SNARE complex by competing with Munc18 for binding syntaxin-1 and thereby negatively regulating neurotransmitter release (Fujita et al., 1998; Sakisaka et al., 2008; Ben-Simon et al., 2015). Mice overexpressing tomosyn in the hippocampus showed impaired spatial learning and memory,

potentially via reduced synaptic transmission in mossy fiber (MF)-CA3 synapses (Barak et al., 2013). Conversely, tomosyn knockout mice exhibited accelerated kindling behaviors due to increased glutamate release in the hippocampal dentate gyrus (Batten SR et al., 2017). Selectively knocking down tomosyn in MF-CA3 synapses also impaired facilitation, long-term potentiation (LTP), and PKA-induced potentiation (Ben-Simon Y et al., 2015). Despite accumulating evidence for the presynaptic roles of tomosyn, a few studies have focused on its role in postsynaptic compartments. One study showed that tomosyn regulates neurite outgrowth in immature neurons by strongly binding to Rho-associated serine/threonine kinase (ROCK)-phosphorylated syntaxin-1 (Sakisaka et al., 2004). Recently, tomosyn has also been shown to regulate dendritic morphology via the ubiquitin-proteasome system (Saldate et al., 2018). We provide evidence showing that tomosyn regulates Rho signaling and the trafficking of glutamate receptors to maintain the structural stability of neurons.

Mechanisms that regulate neuronal stability and synaptic function are often vulnerable targets in neurodevelopmental disorders, such as autism spectrum disorder (ASD) (Hampson and Blatt, 2015; Subramanian et al., 2017; Forrest et al., 2018). Individuals with ASD are characterized by difficulties in social communication and interaction, repetitive behaviors, and restricted interests (American Psychiatric Association, 2013). Although ASD exhibits a high degree of genetic heterogeneity, many identified risk genes converge on similar cellular pathways, including those that regulate neurite outgrowth, spine stability, synaptic plasticity, excitatory/inhibitory balance, and trafficking of glutamate receptors (Oblak et al., 2010, 2011; Iossifov et al., 2014; Sanders et al., 2015; Volk et al., 2015; Chahrour et al., 2016; Lin et al., 2016; Bridi et al., 2017; Short et al., 2018). Several human genetic studies, including genome-wide association studies and whole-exome sequencing, have recently linked the deletion, as well

as two tomosyn variants (L412V and Y502C) to ASD (Davis et al., 2009; Hussman et al., 2011; Matsunami et al., 2013; Cukier et al., 2014). In the present study, reductions of dendritic arborization and spine density accompanied by enhanced RhoA activity and altered surface expression of glutamate receptors were observed in tomosyn knockdown neurons. ASD-associated tomosyn L412V and Y502C variants displayed a loss-of-function effect and failed to restore the cellular defects in tomosyn knockdown neurons. Our study reveals a novel postsynaptic function of tomosyn, which mediates a potential pathway maintaining the structural stability of neurons and may be altered in ASD.

Materials and Methods

Animals. C57BL/6J mice were obtained from the University of Maryland School of Medicine Program in Comparative Medicine. Mice were housed and cared for by the AAALAC accredited program of the University of Maryland School of Medicine. Neonatal mice of both sexes were euthanized for neuronal culture preparation. Hippocampus and whole brain from mice (2 pooled hippocampus and 1 whole brain per age group) of both sexes at different postnatal days (P) P0, P7, P14, and P21 were dissected for Western blot analysis of the temporal expression of tomosyn. Cortex, hippocampus, striatum, and cerebellum from P14 mice (2-3 pooled brain areas per sample) of both sexes were prepared for Western blot analysis of the spatial expression of tomosyn. In addition, forebrains from P21 mice (2 pooled forebrains per sample) were obtained for synaptic fraction analyses. All experiments performed were reviewed and approved by the Institutional Animal Care and Use Committee (IACUC) of the University of Maryland School of Medicine and the Hussman Institute for Autism.

Plasmids. The pcDNA^{TM}4/*myc*-His-m-tomosyn plasmid was a gift from Dr. Sushant Bhatnagar, University of Alabama. The tomosyn-GFP was engineered by adding a green fluorescent protein (GFP) tag at the 3' end of the pcDNA^{TM}4/*myc*-His-m-tomosyn. Short hairpin (shRNA) constructs targeting tomosyn were generated by inserting the anti-tomosyn RNAi (shRNA482 also referred to as shTomosyn-GCACTGAGCGAGGAAACTAC, shRNA1083-GGAACCATATGCTGTGGTTGT) or a scrambled shRNA control (Scramble: CAGGAACGCATAGACGCATGA) into the third generation pLL3.7-RFP vector using the XhoI and HpaI restriction sites as previously described (Ben-Simon et al., 2015). L412V or Y502C point mutation was introduced by site-directed mutagenesis (Agilent Technologies, QuikChange II XL Site-Directed Mutagenesis Kit, Cat# 200521) using pcDNA^{TM}4/*myc*-His-m-tomosyn-GFP plasmid as a template. The shRNA-resistant tomosyn (wild-type WT^{r}-Tom-GFP, L412V^{r}-Tom-GFP, and Y502C^{r} -Tom-GFP) constructs were made by mutating three nucleotides in the shTomosyn sequences with two PCR primers: Forward 5'-AGTGGCTCTATGTGGGCACGGAACGCGGAAACATACACATTGTTA-3' and Reverse 5'-TAACAATGTGTATGTTTCCGCGTTCCGTGCCCACATAGAGCCACT-3'. shTomosyn-WT^{r}-Tom-RFP, shTomosyn-L412V^{r}-Tom-RFP, and shTomosyn-Y502C^{r}-Tom-RFP were generated by inserting WT^{r}-Tom, L412V^{r}-Tom or Y502C^{r}-Tom into the shTomosyn vector. pcDNA3-EGFP-RhoA-WT (Addgene, plasmid # 12965) and pcDNA3-EGFP-RhoA-T19N (Addgene, plasmid # 12967) were a gift from Gary Bokoch (Subauste et al., 2000). pCI-SEP-GluR1 (Addgene, plasmid #24000) was a gift from Robert Malinow (Kopec et al., 2006). pTriEx-RhoA FLARE.sc Biosensor WT (Addgene, plasmid # 12150) was a gift from Klaus Hahn (Pertz et al., 2006). pCAGIG (IRES-GFP) (Addgene, plasmid # 11159) was a gift from

Connie Cepko (Matsuda and Cepko, 2004). pRFP-N1 was constructed by replacing of GFP in the pEGFP-N1 (Clontech, Catalog # 6085-1) with RFP. Full-length (FL) tomosyn and domain-mutant tomosyn with BamHI and EcoRI restriction sites were subcloned into the pRFP-N1 vector. Primer sequences for FL-Tom-RFP: Forward 5'-ATATGAATTCGCCACCATGAGGAAATTCAACATCAG-3' and Reverse 5'-ATATGGATCCATGAACTGGTACCACTTCTTATCTTTG-3'; Tom-ΔC-RFP: Forward 5'-ATATGAATTCGCCACCATGAGGAAATTCAACATCAG-3' and Reverse 5'-ATATGGATCCATGCCCGGGATGTGTTGTG-3'; and Tom-ΔN-RFP: Forward 5'-ATATGAATTCGCCACCATGCCTGGTGGGATC-3' and Reverse 5'-ATATGGATCCATTTTGTATTTCAGCATCATCTCATGAG-3'.

Cell culture and transfections. Neuro-2a (N2a, a mouse neuroblastoma cell line) cells were maintained in high glucose DMEM (Invitrogen) growth media supplemented with 1% penicillin/streptomycin (Invitrogen), 2 mM L-glutamine (Invitrogen), and 10% fetal bovine serum (Sigma-Aldrich). Primary hippocampal cultures were prepared from P0 mice, and plated at a density of 3×10^5 cells/well for morphometric analysis and Förster Resonance Energy ;Transfer (FRET) experiments, or 3×10^4 cells/well for surface staining on 12-mm coverslips in 24-well plates coated with 20 μg/ml poly-(D)-lysine (Sigma-Aldrich). Neurons were maintained in serum-free Neuralbasal^{TM}A media (Invitrogen) containing 1% penicillin/streptomycin, 2 mM L-glutamine, and 2% B27-supplement. Lipofectamine 3000 reagent (Invitrogen, Cat# L3000075) was used to transfect N2a cells according to the manufacturer's protocol. Primary hippocampal neurons were transfected using Lipofectamine 3000 at 4 *days in vitro* (DIV) followed by fixation at 7 DIV for quantifying the dendritic

arborization, and calcium-phosphate transfection method at 11-12 DIV followed by fixation at 15 DIV for spine quantification. For electrophysiological recordings, primary hippocampal neurons were transfected at 9 DIV using Lipofectamine 2000 (Invitrogen, Cat# 11668-027) and incubated until 14-16 DIV.

Inhibition of RhoA signaling. 24 hours after transfection, neurons were either treated with 100 µM of ROCK inhibitor Y-27632 (Millipore Sigma, Cat# 688000) every 24 hours for 48 hours as described previously (Lin et al., 2013), 1.0 µg/mL of RhoA inhibitor C3 transferase (Cytoskeleton, Cat# CT04) for 16 hours, or 10 µL of ddH_2O as a control for 48 hours prior to fixation.

Synaptic fractionation. Synaptic fractionation was prepared as described previously (Bermejo et al., 2014). Briefly, forebrains were homogenized in 4 ml 0.32 M HEPES-buffered sucrose solution (0.32 M sucrose, 4 mM HEPES, 0.25 mM PMSF and protease and phosphatase inhibitors (Thermo Fisher Scientific, Cat# 78442)) at 4 °C by using a motor-driven glass-Teflon tissue homogenizer. Homogenates (total) were centrifuged at 900 × g for 10 minutes at 4 °C to generate the nuclear fraction pellet (P1) and the supernatant (cytosol/membranes, S1). S1 was centrifuged at 10,000 × g for 15 minutes at 4 °C to obtain the crude synaptosomes (P2) and the supernatant (cytosol/light membranes, S2). P2 was washed with 0.32 M HEPES-buffered sucrose solution and re-centrifuged at 10,000 × g for 15 minutes at 4 °C. P2', obtained from P2, was lysed in 4 ml ddH_2O by hypoosmotic shock, and was adjusted back to 4 mM HEPES. P2' lysate was centrifuged at 25,000 × g for 20 minutes at 4 °C to isolate the synaptosomal membrane fraction (synaptosomes, P3) in the pellet and the crude vesicular fraction in the supernatant

(synaptic vesicles, S3). P3 in 1 ml of 0.32 M HEPES-buffered sucrose solution was loaded on discontinuous sucrose gradient and re-centrifuged at 150,000 × g for 2 hours at 4 °C to obtain synaptic plasma membranes (SPM). SPM was re-suspended in Triton X-100/HEPES/EDTA solution (0.54% Triton X-100, 50 mM HEPES, 2 mM EDTA) and centrifuged at 32,000 × g for 20 minutes at 4 °C to obtain the post-synaptic density fraction (PSD). A total of 10 µg proteins from each fractionation were loaded for Western blot analysis.

Western blot analysis. Brain tissues or N2a cells transfected with plasmids were harvested in RIPA buffer containing 20 mM Tris-HCl (pH 7.5), 150 mM NaCl, 1 mM Na_2EDTA, 1 mM EGTA, 1% NP-40, 1% sodium deoxycholate, 2.5 mM sodium pyrophosphate, 1 mM beta-glycerophosphate, 1 mM Na_3VO_4, 1 µg/ml leupeptin, 1 mM PMSF, and a phosphatase and protease inhibitor cocktail (Sigma-Aldrich, Cat# MSSAFE). Protein concentration was determined using a Pierce BCA Protein Assay Kit (Thermo Fisher Scientific, Cat# 23227). A total of 50 µg protein from N2a cell lysates were used to determine the knockdown efficiency of tomosyn shRNAs. A total of 10 µg protein from different brain regions were used to examine tomosyn expression. Protein samples were run on 8% gels for SDS-PAGE and transferred to a PVDF membrane. After blocking the membrane with 5% skim milk in TBST (0.1% Tween 20 in TBS) for 1 hour at room temperature, the membrane was immunoblotted with the following primary antibodies: rabbit anti-tomosyn (1:1000, Synaptic Systems, Cat# 183103, RRID: AB_2619878), mouse anti-β-Actin (1:5000, Sigma-Aldrich, Cat# A1978, RRID: AB_476692), mouse anti-syntaxin-1a (1:1000, Synaptic Systems Cat# 110111, RRID:AB_887848), mouse anti-syntaxin-4 (1:1000, Synaptic Systems, Cat# 110041, RRID: AB_11042324), mouse anti-SNAP-25 (1:1000, Synaptic Systems, Cat# 111011, RRID:AB_887794), rabbit anti-SNAP-23

(1:1000, Synaptic Systems, Cat# 111203, RRID:AB_887787), mouse anti-PSD-95 (1:1000, UC Davis/NIH NeuroMab Facility, Cat# 75-028, RRID:AB_2307331), and mouse anti-c-Myc (1:3000, Sigma-Aldrich, Cat# M4439, RRID:AB_439694). The membrane was washed 3 times with TBST for 10 minutes and incubated with the HRP-conjugated secondary antibodies for 60 minutes at room temperature. The membrane was then washed 5 times with TBST for 10 minutes at room temperature. The chemiluminescent blots were imaged with the ChemiDoc™ Touch Imaging System (Bio-Rad). The densitometry of the protein signals was analyzed using Image Lab™ software (Bio-Rad).

Immunoprecipitation. Immunoprecipitations of endogenous binding partners of tomosyn or syntaxin-4 were performed using lysates of cultured cortical neurons. Cultured cortical neurons were lysed in lysis buffer (20 mM Tris, pH 7.5, 150 mM NaCl, 1% Triton X-100) containing phosphatase and protease inhibitor cocktail (Thermo Fisher Scientific, Cat# 78442). Lysates were precleared with protein A/G agarose beads (Thermo Fisher Scientific, Cat# 20421) for 1 hour. 2 µg of rabbit anti-tomosyn or mouse anti-syntaxin-4 antibody was added to the lysate followed by rotation overnight at 4 °C. 20 µL of protein A/G agarose was added to the immune complex and incubated for 1 hour at 4 °C. The beads were washed five times with TBST. Bound proteins were eluted in 2 × Laemmli sample buffer (Bio-Rad, Cat# 161-0737) containing 5% 2-mercaptoethanol by heating at 95 °C for 5 minutes. Immunoprecipitations of tagged-tomosyn proteins were performed using N2a cells. Transfected N2a cells were lysed in IP lysis buffer (Thermo Fisher Scientific, Cat# 1861603) (25 mM Tris, 150 mM NaCl, 1 mM EDTA, 1% NP-40, 5% glycerol, pH 7.4) containing a phosphatase and protease inhibitor cocktail and 1 mM PMSF. Protein concentrations were measured using BCA assay. 500 µg of proteins were used

for c-Myc-tagged tomosyn co-immunoprecipitation (Thermo Fisher Scientific, ProFound™ c-Myc Tag IP/Co-IP Application Set, Cat# 23622). Following the manufacturer's instructions, protein lysates were precleared with the protein A/G agarose. 10 µL of anti-c-Myc agarose was added to the precleared lysate followed by end-over-end rotation overnight at 4 °C. The agarose beads were washed five times with TBST, and bound proteins (syntaxin-1 and syntaxin-4) were eluted from beads using 2× Laemmli sample buffer containing 5% 2-mercaptoethanol by heating at 95 °C for 5 minutes. Other bound proteins (SNAP-23 and SNAP-25) were eluted using a low pH elution buffer (pH 2.0) and then neutralized by 1 M Tris, pH 9.5.

Immunocytochemistry and morphometric analysis. Cultured neurons were fixed at 7 or 15 DIV with 4% paraformaldehyde in phosphate buffer (PB) (320 mM Na_2HPO4, 76 mM NaH_2PO4) for 15 minutes and permeabilized and blocked in TBS containing 0.1% Triton X-100, 3% BSA and 1% donkey serum. Cells were immunostained with the following primary antibodies: mouse anti-GFP (1:5000, Molecular Probes, Cat# A-11120, RRID: AB_221568), rat anti-RFP (1:1000, Chromotek, Cat# 5f8-100, RRID: AB_2336064), rabbit anti-tomosyn (1:500, Synaptic Systems, Cat# 183103, RRID: AB_2619878), mouse anti-MAP2 (1:2000, Sigma-Aldrich, Cat# M9942, RRID: AB_477256), mouse anti-CaMKIIα (1:500, Thermo Fisher Scientific, Cat# MA-048, RRID: AB_325403), and mouse anti-GAD67 (1:500, Millipore Sigma, Cat# MAB5406, RRID: AB_2278725) followed by Alexa Fluor 488, 568, 594-conjugated secondary antibodies (Invitrogen). For dendrite analysis, z-stack images were taken using a confocal laser scanning microscope (Zeiss LSM 780) with a 40 X/1.3 oil DIC objective. Original images of neurons were used to trace dendrites for dendrite length measurement using ImageJ (NIH) with NeuronJ plugin (Meijering et al., 2004). Traced neurons were further analyzed using ImageJ with Sholl analysis

plugin (Ferreira et al., 2014). Concentric circles having 10 µm increments in radius were defined from the center of cell body. The number of traced dendrites crossing each circle was counted. For spine analysis, 2–3 dendrite segments per neuron were selected randomly from secondary branches on the apical dendrite. Z-stack images were taken using Zeiss LSM 780 with a 63 ×/1.4 oil DIC objective and 4 zoom at 512 × 512 resolution. The number of dendritic spines, which is ≤ 2 µm in length, were manually counted using ImageJ. Images of neurons co-immunostained with either CaMKIIα or GAD67 and tomosyn were taken using EVOS FL Auto2 imaging system with a 40 ×/0.95 NA air objective (Invitrogen).

Surface staining. Neurons were co-transfected pCI-SEP-pHluorin-GluR1 (Addgene, plasmid # 24000) with either scrambled shRNA or shTomosyn. The surface staining of pHluorin-GluR1 was performed as previously described (Noel et al., 1999; Gu et al., 2016). Briefly, transfected neurons were incubated with mouse anti-GFP antibody in pre-chilled artificial cerebrospinal fluid (ACSF) (124 mM Nacl, 5 mM KCl, 1.23 mM NaH_2PO_4, 26 mM $NaHCO_3$, 1 mM $MgCl_2$, 2 mM $CaCl_2$,) containing 10% BSA for 1 hour at room temperature. Cells were washed three times with ACSF, incubated with donkey anti-mouse Alex Fluor 647-conjugated secondary antibody (1:1000, Invitrogen) for 1 hour at room temperature, and again washed three times with ACSF. For total pHluorin-GluR1 staining, cells were fixed with 4% paraformaldehyde in PB for 15 minutes, permeabilized, and blocked in blocking solution. Cells were immunostained with rabbit anti-GFP (1: 4000, Antibodies-Online, Cat# ABIN346939, RRID: AB_10820004) and rat anti-RFP antibodies. Cells were washed three times followed by incubation with goat anti-rat Alexa Fluor 568- and donkey anti-rabbit Alexa Fluor 488-conjugated secondary antibody. Coverslips were mounted on the glass slides with Prolong Diamond Antifade Mountant (Molecular Probes,

Cat# P36961) prior to imaging. 2–3 dendrite segments per neuron were selected randomly from secondary branches on the apical dendrite. Identical acquisition settings were applied to each image within all experiments. For surface GluR1 expression quantification, surface GluR1/total GluR1 was calculated as surface/total = (mean intensity of surface- background intensity) / (mean intensity of total-background intensity).

FRET analysis. Hippocampal neurons were co-transfected with pTriEx-RhoA FLARE.sc Biosensor WT and either scrambled shRNA or shTomosyn at 4 DIV. Cells were fixed with 4% paraformaldehyde in PB and mounted at 7 DIV. Imaging was performed with an upright Zeiss confocal LSM 780 and a 40× EC Plan-NeoFluar/1.3 oil-immersion objective lens. For sensitized emission, FRET excitation was performed using the 458 nm laser, and emission filter bands were set to 440-510 for CFP and 517-606 for YFP. The 561 nm laser was used for excitation of RFP to identify shRNA-transfected neurons. Single plane images were exported to ImageJ for analysis. The RFP channel image was used as a reference to create a whole cell ROI (region-of-interest), which was subsequently overlaid on CFP and YFP channel images and mean fluorescence intensity (I) was measured within the ROI. As the RhoA-FLARE is an intramolecular FRET biosensor, the FRET efficiency (E_{FRET}) is calculated by simple ratiometry of acceptor (YFP) over donor (CFP) intensity: $E_{FRET} = I_{YFP}/I_{CFP}$. Acceptor photobleaching FRET was done by placing a circular bleach ROI (r = 2.04 μm) over secondary or tertiary parts of either apical or basal dendritic compartments of transfected neurons. Acceptor bleaching was executed over 50 iterations with the 514 nm laser at maximum power. Changes in fluorescence intensities in the donor (CFP) and acceptor (YFP) channels were recorded using low power (2%) excitation with the 458 nm and 514 nm lasers, respectively, and a total of 10 scans were

acquired: 5 before (pre) and 5 after (post) the single bleaching event. The mean fluorescence intensity values (I) of ROIs were exported to Excel. The donor channel bleach ROI data was background corrected and normalized to unbleached background ROIs and reference ROIs, respectively. FRET efficiency (E_{FRET}) in percentage was calculated according to: $E_{FRET} = ((Idonor_{post} - Idonor_{pre}) / Idonor_{post}) \times 100$. All calculated E_{FRET} data was exported to GraphPad Prism 6 for statistical analysis.

Electrophysiology. Neurons at 14-16 DIV were used for whole-cell electrophysiological recordings following either scrambled shRNA or shTomosyn transfection at 9 DIV. Coverslips were transferred from a 24-well plate into a recording chamber superfused with a buffer containing the following (in mM): 125 NaCl, 3 KCl, 10 HEPES, 5 dextrose, 1 $MgCl_2$, and 2 $CaCl_2$. The recording buffer was adjusted to ~260 mOsm and pH 7.2, and the bath was maintained at a temperature of 30°C. Glass pipettes pulled to a resistance of 3-7 MΩ were filled with internal solution containing the following (in mM): 134 KMeSO4, 3 KCl, 10 HEPES, 1 $MgCl_2$, 4 MgATP, 0.5 Na_2GTP, 5 K_2-creatine phosphate, and 5 Na_2-creatine phosphate. Internal solution was adjusted to ~250 mOsm and pH 7.4. Only RFP-expressing cells with a series resistance ≤ 30 MΩ and a resting membrane potential ≤ -50 mV were accepted for final analysis. Whole-cell parameters were monitored throughout the recording with a 100 ms, -10 mV step delivered every 30 seconds. Recordings were made using an Axon MultiClamp 700B amplifier (Molecular Devices). Data were filtered at 2 kHz and digitized at 10 kHz with a National Instruments digital-analog converter under the control of Igor Pro software (WaveMetrics). Miniature EPSCs were recorded in voltage mode (Vh = -70 mV) in the presence of 50 µM AP5, 1 µM tetrodotoxin (TTX), and 10 µM gabazine (GBZ). The frequency, amplitude, and kinetics

of mEPSCs were analyzed with Mini Analysis software (Synaptosoft), with a threshold of 3 × RMS noise for event discrimination. At least 50 events per cell were used in these calculations.

Experimental design and statistical analysis. Sample sizes for each experiment are based on previously published studies from our laboratory and standards in the field. Values were expressed as mean ± SEM (standard error of the mean). n = number of neurons or repeats. All statistical comparisons were performed using GraphPad Prism 6 (GraphPad Software, San Diego, CA). Variable comparisons between groups were performed using either one-way ANOVA with Dunnett's *post hoc* test or two-way ANOVA with Tukey's or Sidak's *post hoc* test. P-values smaller than 0.05 were considered significant.

Results

Tomosyn is expressed at pre- and post-synaptic areas

Protein expression of tomosyn in developing mouse brains was first determined using Western blot analysis. The expression of tomosyn in whole brain was readily detectable from P0 and increased temporally during development (Fig.1*A*). Spatial analysis revealed a dominant expression profile of tomosyn in the forebrain compared to the cerebellum (Fig. 1*B*). Further examination in the hippocampus showed that the protein level of tomosyn increased nearly four-fold by P14 compared to P0 (Fig. 1*C*). Similarly, tomosyn expression increased with PSD-95 in cultured cortical neurons, suggesting a role in synaptogenesis. To determine the subcellular localization of tomosyn, cultured hippocampal neurons were co-immunostained with tomosyn and microtubule-associated protein 2 (MAP2), which is the dendritic marker. Endogenous tomosyn was shown to localize in both the soma and MAP2-positive dendrites (Fig. 1*E*).

Overexpressed tomosyn-GFP also localized in the dendritic compartments, including dendritic spines (Fig. 1*F*). The expression level of tomosyn in dendritic spines was similar to dendrite shafts (Fig. 1*G*). Synaptic fractionation analysis of the forebrain further confirmed the postsynaptic localization of tomosyn (Fig. 1*H*). Tomosyn was enriched in pre-synaptic compartments including syntaxin-1-rich synaptic plasma membrane (SPM) and synaptic vesicles (S3). However, tomosyn was also detected in the postsynaptic density (PSD), which was indicated by the strong presence of PSD-95. In addition, immunofluorescence labeling of cultured hippocampal neurons further revealed tomosyn expression in both CaMKIIα-positive excitatory neurons and GAD67-positive inhibitory neurons (Fig. 1*I*). These data establish the spatiotemporal expression pattern of tomosyn in the brain, and suggest a role in dendritic development.

Knockdown of tomosyn decreases dendritic complexity and dendritic spine density

To examine the effect of tomosyn on neuronal morphology, a short hairpin RNA (shRNA) expression system was used to knock down tomosyn in cultured hippocampal neurons. The knockdown efficiency of two shRNAs targeting tomosyn, shRNA482 and shRNA1083, was first determined in N2a cells. shRNA482 and shRNA1083 resulted in 87.9% and 79.3% reduction, respectively, in the amount of overexpressing GFP-tagged tomosyn protein compared to scrambled shRNA ($F_{(2, 6)} = 85.74$, $p = 3.8 \times 10^{-5}$) (Fig. 2*A*). shRNA482, which most effectively decreased tomosyn expression, was chosen for the following experiments and is referred to as shTomosyn hereafter. To further evaluate the knockdown specificity of shTomosyn, an shRNA-resistant form of tomosyn was engineered as Tom^r-GFP. Co-expressing Tom^r-GFP with

shTomosyn effectively restored the protein level of tomosyn back to control levels ($F_{(2, 6)} = 20.14$, $p = 0.0022$) (Fig. 2*B*).

To determine whether tomosyn plays a role in neuronal morphogenesis, shTomosyn was used to knock down tomosyn expression in cultured hippocampal neurons, and their dendritic arborization was first examined. Reconstructions of dendritic trees (Fig. 2*C*) and Sholl analysis (Fig. 2*D*) showed that the overall size of the dendritic arbors was smaller in tomosyn knockdown neurons. Co-expression of Tom^r-GFP efficiently restored dendritic complexity within the first 100 μm radius of dendritic arbors in knockdown neurons ($F_{(2, 1750)} = 02.4$, $p = 8.8 \times 10^{-43}$). Knockdown of tomosyn also resulted in decreased spine density (scramble: 0.61 ± 0.02 /μm; shTomosyn: 0.36 ± 0.02 /μm), while re-expressing Tom^r-GFP (0.53 ± 0.02 /μm) successfully rescued dendritic spine loss ($F_{(2, 179)} = 69.95$, $p = 3.5 \times 10^{-23}$) (Fig. 2*E* and *F*). Together, these data suggest that tomosyn plays a role in regulating dendritic arborization and spine stability.

Tomosyn deficiency leads to reduced frequency of mEPSCs

Because tomosyn deficiency results in abnormal dendritic arborization and spinogenesis, this raised a critical question about the postsynaptic role of tomosyn in maintaining basal excitatory synaptic transmission. To address this issue, the effect of tomosyn knockdown on miniature AMPA receptor (AMPAR)-mediated EPSCs (mEPSCs) in cultured hippocampal neurons was examined. Miniature EPSC frequency (Fig. 3*C*, scramble: 5.18 ± 0.78 Hz, shTomosyn: 1.46 ± 0.36 Hz, $p = 3.8 \times 10^{-5}$) was significantly reduced in tomosyn knockdown cells compared to controls. Charge (Fig. 3*E*, scramble: 42.41 ± 3.61, shTomosyn: 32.89 ± 2.23, $p = 0.03$), but not amplitude (Fig. 3*D*, scramble: 16.35 ± 1.46 pA, shTomosyn: 14.55 ± 1.01 pA, $p = 0.31$), was decreased in tomosyn knockdown neurons compared to scrambled shRNA transfected neurons.

Analysis of mEPSC kinetics found that the decay time constant ($p = 0.01$) was significantly smaller in tomosyn knockdown neurons than in the scramble controls. These data showing a reduction of mEPSC frequency support the spine loss phenotype observed in tomosyn knockdown neurons, while the attenuation in the decay time constant may indicate a change in AMPAR subunit composition at the synapse in shTomosyn cells.

Tomosyn knockdown leads to elevated RhoA GTPase activity

Decreased dendritic arborization and destabilization of dendritic spines on pyramidal neurons have previously been linked to the increased activity of RhoA GTPase (Nakayama et al., 2000). Thus, we investigated whether simplification of dendritic arbors and loss of dendritic spines observed in neurons with tomosyn knockdown were the result of elevated RhoA activity. Hippocampal neurons were co-transfected with either scrambled shRNA or shTomosyn, as well as an intramolecular FRET RhoA biosensor, which contains the CFP (donor)/YFP (acceptor) FRET pair flanked on one side by full-length RhoA, and the Rho-binding domain of the effector rhotekin (RBD) on the other (Pertz et al., 2006). Upon activation of RhoA, the RBD element associates with RhoA-GTP, thereby causing the biosensor molecule to change its conformation into a FRET-favorable state. Hence, RhoA activity can be monitored by measuring the FRET occurring between the CFP and YFP fluorophores (Pertz et al., 2006; Aoki and Matsuda, 2009). FRET efficiency was recorded by two different well-established techniques: sensitized emission (Fig. 4*A* and *B*) and acceptor photobleaching (Fig. 4*C, C'* and *D*). RhoA biosensor FRET signal recorded by sensitized emission revealed that knockdown of tomosyn resulted in a significantly higher FRET ratio compared to scramble control ($p = 0.0286$) (Fig. 4*A* and *B*). Similarly, acceptor (YFP) photobleaching FRET (pbFRET) performed at selected regions along apical and

basal dendrites showed that overall E_{FRET} was greater in tomosyn knockdown neurons compared to scramble control ($F_{(1, 57)} = 31.05$, $p = 7.1 \times 10^{-7}$) (Fig. 4*C, C'*and *D*). However, within each sample group (scramble and shTomosyn) no significant differences in E_{FRET} were observed between the specified dendritic compartments ($F_{(1, 57)} = 0.0093$, $p = 0.9234$). Collectively, these data show that RhoA activity is increased in tomosyn knockdown neurons, indicating that tomosyn might play a role in the maintenance of dendritic morphology by regulating RhoA GTPase signaling. To further investigate which part of tomosyn is essential for inhibiting RhoA activity, two domain mutants were constructed: Tom-ΔC-RFP, which contains the N-terminal WD40 domain, and Tom-ΔN-RFP, which contains only the R-SNARE domain of tomosyn (Fig. 4*E*). Western blot analysis showed that both Tom-ΔC-RFP and Tom-ΔN-RFP migrated as shorter versions of tomosyn at the predicted size (Fig. 4*F*). FRET analysis showed that RhoA activity in neurons expressing Tom-ΔC-RFP is comparable to that of RFP control and full-length tomosyn. However, E_{FRET} was significantly increased in neurons expressing Tom-ΔN-RFP ($F_{(3,117)} = 36.81$, $p = 7.9 \times 10^{-17}$) (Fig. 4*G*), suggesting lack of the WD40 domain of tomosyn is sufficient for increasing RhoA activity (Fig. 4*G*). Taken together, these data suggest that tomosyn likely functions as a negative regulator for RhoA activity via the WD40 domain in neurons.

Inhibition of RhoA signaling restores dendritic arborization and spine density in tomosyn-deficient neurons

To determine whether inhibiting RhoA activity is sufficient to rescue the aberrant dendritic phenotypes in tomosyn knockdown neurons, dominant-negative RhoA (T19N-RhoA) was co-transfected in scramble control- and shTomosyn-expressing neurons. As shown earlier, tomosyn

knockdown neurons exhibited less dendritic complexity measured by total dendrite length (scramble: 1092.62 ± 65.77 µm, shTomosyn: 742.84 ± 50.23 µm, $p = 1.4 \times 10^{-5}$), branch number (scramble: 23.4 ± 1.5, shTomosyn: 16.2 ± 1.0, $p = 8.9\times 10^{-6}$), and spine density (scramble: 0.46 ± 0.03 μm^{-1}, shTomosyn: 0.33 ± 0.02 μm^{-1}, $p = 0.005$). When T19N-RhoA was expressed, tomosyn knockdown neurons showed similar total dendrite length (Fig. 5*A-C*) (scramble: 1163.67 ± 39.92 µm, shTomosyn: 1067.38 ± 49.17 µm, $p = 0.48$), branch number (scramble: 21.5 ± 1.0, shTomosyn: 20.0 ± 1.1, $p = 0.6684$) and spine density (scramble: 0.47 ± 0.03 μm^{-1}, shTomosyn: 0.53 ± 0.03 μm^{-1}, $p = 0.294$) compared to control neurons. In contrast, overexpression of WT-RhoA did not affect the compromised dendritic morphology of tomosyn knockdown neurons (Fig. 5*A-C*) (total dendrite length—scramble: 1169.43 ± 64.79 µm, shTomosyn: 774.95 ± 48.83 µm, $p =2.8 \times 10^{-7}$; branch number—scramble: 20.7 ± 1.1, shTomosyn: 15.3 ± 0.7, $p = 0.001$; spine density—scramble: 0.48 ± 0.02 μm^{-1}, shTomosyn: 0.34 ± 0.02 μm^{-1}, $p = 0.0003$). Treating cultured neurons with C3T, a RhoA inhibitor, also fully rescued the dendritic phenotypes in tomosyn knockdown neurons (Fig. 5*D-F*) (total dendrite length—scramble: 938.83 ± 41.6 µm, shTomosyn: 901.65 ± 49.91 µm, $p = 0.925$; branch number—scramble: 19.7 ± 1.1, shTomosyn: 19.5 ± 1.3, $p = 0.999$; spine density—scramble: 0.53 ± 0.03 μm^{-1}, shTomosyn: 0.52 ± 0.02 μm^{-1}, $p = 0.964$). Inhibiting ROCK, the downstream effector of RhoA, with Y-27632 only rescued the total dendrite length (Fig. 5*D*) (scramble: 996.89 ± 50.92 µm, shTomosyn: 956.28 ± 51.31 µm, $p = 0.927$) and branch number (Fig. 5*E*) (scramble: 21.1 ± 1.0, shTomosyn: 19.9 ± 1.3, $p = 0.881$). However, the reduced spine density in tomosyn knockdown neurons was not rescued by Y-27632 treatment (Fig. 5*F*) (scramble: 0.42 ± 0.03 μm^{-1}, shTomosyn: 0.30 ± 0.02 μm^{-1}, $p = 0.0016$). This data suggest that tomosyn may

regulate dendritic arborization through RhoA and ROCK inhibition, but may act through a different mechanism other than ROCK to regulate the stability of dendritic spines.

Knockdown of tomosyn leads to altered surface-expressed glutamate receptors

Since C3T, but not Y-27632, restored decreased spine density in tomosyn knockdown neurons, it prompted us to investigate another potential mechanism mediated by tomosyn for spine density maintenance. Alterations in the surface expression of glutamate receptors mediated by dendritic SNARE fusion machinery often result in changes in spine structures and synaptic plasticity (Henley and Wilkinson, 2016; Reiner and Levitz, 2018). Previous studies have shown that tomosyn forms a complex with syntaxin-4 in non-neuronal cells to mediate exocytosis (Widberg et al., 2003; Zhu et al., 2014). Syntaxin-4, as a postsynaptic t-SNARE, previously has been shown to regulate AMPAR trafficking in LTP (Kennedy et al., 2010). We predicted that tomosyn may interact with syntaxin-4 and other dendritic SNARE molecules, such as SNAP-25 and SNAP-23, in neurons to regulate the structural stability of spines. Here, interaction between tomosyn and syntaxin-4 in neurons was examined. Co-immunoprecipitation of endogenous tomosyn and syntaxin-4 in cultured cortical neurons was detected by using either tomosyn or syntaxin-4 as the bait antibody to pull down the other (Fig. 6*A*). To further evaluate whether the expression of syntaxin-4 was affected by tomosyn downregulation, the protein level of syntaxin-4 was determined in tomosyn knockdown N2a cells. While shTomosyn reduced endogenous tomosyn expression by 48.4% ($F_{(1, 16)} = 118.3$, $p = 8.42 \times 10^{-7}$), syntaxin-4 expression was not affected (Fig. 6*B*). However, knocking down tomosyn led to decreased fluorescent signals from pHluorin-GluR1 on dendritic surfaces. Interestingly, total GluR1 receptor fluorescence in tomosyn knockdown neurons remained highly punctate in distribution along dendrites, but no

difference of total mean intensity was found compared to control neurons ($p = 0.191$ by two-tailed Mann-Whitney U test, graph is not shown) (Fig. 6*C*). Given that tomosyn interacts with syntaxin-4, and RhoA signaling is involved in AMPA receptor trafficking (Kang et al., 2009), we hypothesized that tomosyn has a role in linking RhoA signaling and AMPAR surface expression. To next address whether inhibition of RhoA activity influences trafficking of glutamate receptors in tomosyn-deficient neurons, the surface expression of the AMPA receptor GluR1 subunit was measured. Treatment with C3T significantly restored the surface expression of GluR1 in tomosyn knockdown neurons back to the control levels ($F_{(2, 108)} = 4.25$, $p = 0.01$) (Fig. 6*D*). Together, these results suggest that tomosyn interacts with syntaxin-4 in neurons and controls AMPA receptor trafficking via RhoA inactivation.

Autism-associated tomosyn variants fail to maintain dendritic complexity and exhibit increased RhoA activity

Recently, two tomosyn variants harboring missense mutations (L412V and Y502C) in the N-terminal WD40 domain have been identified in individuals with autism (Cukier et al., 2014) (Fig. 7*A*). The experiments performed in the present study showed that tomosyn may act as a negative regulator of RhoA and that the inhibitory function is likely mediated by the WD40 domain (Fig. 4). To evaluate whether the two autism-associated tomosyn variants disrupt their inhibitory function on RhoA, shRNA-resistant forms of two tomosyn variants, L412V^r-Tom-GFP and Y502C^r-Tom-GFP, were engineered. When co-expressed with shTomosyn, WT^r-Tom-GFP, L412V^r-Tom-GFP, and Y502C^r-Tom-GFP all effectively rescued the protein level of tomosyn back to control ($F_{(4.10)} = 10.83$, $p = 0.0012$) (Fig. 7*B*). RhoA activity was determined using the FRET biosensor analysis. A significant increase in FRET signals was detected in

neurons expressing L412V ($p = 0.0051$) or Y502C variants ($p = 0.0106$) compared to those expressing WT tomosyn (Fig. 7*C*). When dendritic morphology was measured, variants displayed a defect to restore the complexity of dendritic arbors or spine density (Fig. 7*D-H*). As previously shown, knockdown of tomosyn caused a reduction of dendritic arbors in total length (scramble: 1348.64 ± 104.85 µm, shTomosyn: 771.38 ± 48.58 µm, $p = 6.54 \times 10^{-6}$) and branch number (scramble: 24.33 ± 1.6, shTomosyn: 17.09 ± 1.3, $p = 0.001$) in comparison with scramble control. WT^{r}-Tom-GFP rescued the decrease in total dendrite length (1252.15 ± 60.11 µm, $p = 0.7218$, vs. scramble) and branch number (22.84 ± 1.2, $p = 0.016$, $p = 0.8730$, vs. scramble), whereas cells co-expressing with L412V^{r}-Tom-GFP or Y502C^{r}-Tom-GFP still showed simplified dendritic morphology: total length (L412V: 960.7 ± 51.31 µm, $p = 0.0002$, vs. scramble; Y502C: 865.03 ± 53.11 µm, $p < 0.0001$, vs. scramble), branch number (L412V: 21.38 ± 1.3, $p = 0.3318$, vs. scramble; Y502C: 18.53 ± 1.4, $p = 0.0118$, vs. scramble) (Fig.7*D-F*). Similarly, a decrease in dendritic spine density was observed as previously shown in tomosyn knockdown neurons (0.37 ± 0.022 /µm) compared to control neurons (0.613 ± 0.022 /µm), ($F_{(4, 307)} = 42.39$, $p = 2.6 \times 10^{-28}$). Co-expression of shTomosyn and WT^{r}-Tom-GFP (0.53 ± 0.022 /µm, $p = 1.7 \times 10^{-10}$) or Y502C^{r}-Tom-GFP (0.46 ± 0.022 /µm, $p = 0.005$) rescued spine loss compared to tomosyn knockdown neurons. Conversely, a reduction in spine density (0.39 ± 0.021 /µm, $p = 3.6 \times 10^{-21}$, vs. scramble) was found in neurons co-expressing shTomosyn and L412V^{r}-Tom-GFP (Fig. 7*G-H*). These data suggest that tomosyn with L412V or Y502C mutation produces a loss-of-function effect for the maintenance of dendritic structures through Rho signaling.

Autism-associated tomosyn variants cause a decrease in surface expression of GluR1

Given that tomosyn is involved in the trafficking of GluR1 via interactions with dendritic SNARE proteins (Fig. 6), the interaction and function of the two autism-associated tomosyn variants with dendritic SNARE molecules were next examined. The c-Myc-tagged WT, L412V or Y502C-Tom constructs were overexpressed and immunoprecipitated from N2a cells. The level of the co-immunoprecipitated SNARE proteins, including syntaxin-1, syntaxin-4, SNAP-25, and SNAP-23 from cells expressing L412V or Y502C-Tom were quantified and relative to the level from cells expressing WT-Tom. L412V- and Y502C-Tom immunoprecipitated syntaxin-1 ($F_{(2.6)} = 0.0035$, $p = 0.9965$) and SNAP-23 ($F_{(2.6)} = 0.3309$, $p = 0.37$) at levels comparable to WT-Tom (Fig. 8*A* and *D*). Intriguingly, both L412V- and Y502C-Tom bound significantly more to syntaxin-4 compared to WT-Tom ($F_{(2.6)} = 4.9$, $p = 0.0329$) (Fig. 8 *B*). L412V-Tom showed increased binding to SNAP-25, whereas Y502C-Tom bound less to SNAP-25 compared to WT-Tom ($F_{(2.6)} = 13.17$, $p = 0.0064$) (Fig. 8 *C*). These data suggest that tomosyn carrying L412V or Y502C mutation interacts differently with dendritic SNARE proteins. The surface expression of GluR1 was further examined to determine whether trafficking of glutamate receptors is affected by these two mutations. Remarkably, neurons expressing L412V^r-Tom, but not Y502C^r-Tom, showed the same phenotype as neurons expressing shTomosyn, displaying a highly punctate distribution of total GluR1 (Fig. 8 *E and F*). Additionally, decreased GluR1 surface expression was detected in neurons rescued with L412V^r-Tom compared to neurons rescued with WT^r-Tom ($p = 0.0063$), whereas Y502C^r-Tom restored the surface expression of GluR1 to levels similar to rescue with WT^r-Tom ($p = 0.2725$). Taken together, these data suggest that L412 mutation in tomosyn may affect GluR1 surface expression via increased binding to syntaxin-4 and SNAP-25 while Y502C mutation has a milder effect.

Discussion

The role of tomosyn in regulating neurotransmitter release and exocytosis in non-neuronal cells has been extensively studied (Ashery et al., 2009; Ye et al., 2014; Zhu et al., 2014; Batten et al., 2017; Madera-Salcedo et al., 2018). Because tomosyn is also distributed throughout dendrites (Fujita et al., 1998; Barak et al., 2010), an undiscovered role in postsynaptic function is likely present. Here, we described the presence and function of tomosyn in postsynaptic areas. We have shown that tomosyn is a novel link between neuronal stability and transmission, which acts as an inhibitory regulator of RhoA GTPase and plays a positive role in AMPA receptor trafficking in neurons. Autism-associated tomosyn variants L412V and Y502C showed a loss-of-function effect, causing spine loss and simplified dendritic arborization accompanied by different degree of GluR1 surface expression when compared to WT controls. Furthermore, our study provides insights into a putative mechanism mediated by RhoA signaling to alter neuronal stability in tomosyn-associated autism.

The expression of tomosyn has been shown in several brain regions using *in situ* hybridization and immunohistochemistry (Groffen et al., 2005; Barak et al., 2010). However, its spatiotemporal expression profile and subcellular localization have not yet been fully studied. Using biochemical approaches, we further revealed that tomosyn is widely expressed in multiple brain regions, including the cerebral cortex, hippocampus, thalamus, striatum, and cerebellum. Tomosyn is present in both CaMKIIα-positive excitatory neurons and GAD67-positive inhibitory neurons. We also showed that the protein level of tomosyn is developmentally regulated. Consistent with previous studies examining mRNA expression, the protein level of tomosyn peaks at P14 in mouse brains, which is equivalent to early childhood in humans (Groffen et al., 2005; Li et al., 2017). These findings suggest that tomosyn may play an

important role during brain development. Our further subcellular examinations revealed that tomosyn was detected in both PSD fractions and in presynaptic areas. The changes in neuronal morphology and basal neurotransmission upon tomosyn knockdown also showed that tomosyn exhibits a cell-autonomous effect on dendritic structures and synaptic activity. Our findings demonstrate the detailed expression profile of tomosyn in the developing brain, and indicate an essential role for tomosyn in the maintenance of dendritic arborization, spine density, and basal neurotransmission.

Previous studies have indicated that tomosyn, containing WD40 repeats, shows significant sequence similarity to lethal (2) giant larvae (L2gl) and yeast protein Sro7p (Mechler et al., 1985; Lehman et al., 1999). The WD40 domain is a scaffolding structure involved in small GTPase-mediated protein-protein interaction (Schapira et al., 2017). Interaction of Sro7p and Sec4p Rab GTPase is implicated in Rab GTPase-dependent vesicle clustering and tethering (Rossi et al., 2015; Rossi et al., 2018). Sro7p has also been reported to disrupt cell polarity via suppression of a small GTPase Rho3p (Kagami et al., 1998). Similar to the yeast homologue, tomosyn has recently been shown to interact with the GTP-bound state of Rab3A to partition synaptic vesicle pools (Cazares et al., 2016). All of this evidence suggests that tomosyn may interact with small Rho GTPases via the WD40 domain. FRET analysis in the current study revealed an increase of RhoA activity in tomosyn knockdown neurons. Domain analysis further indicated that the N-terminus of tomosyn with its WD40 repeats is likely responsible for mediating this RhoA inhibition. However, more sophisticated biochemical studies are required for further understanding this inter-molecular regulation.

Pharmacologically inhibiting RhoA or ROCK restored the simplified dendritic arbors in tomosyn knockdown neurons. However, while RhoA inhibition restored the decreased spine

density in tomosyn-downregulated neurons, ROCK inhibition did not. These data suggest that dendritic arborization is mediated by pathways involving RhoA and ROCK, while the stability of dendritic spines may require mechanisms other than ROCK. Alterations in the trafficking of glutamate receptors also lead to structural changes in dendritic spines and synaptic plasticity (Henley and Wilkinson, 2016; Reiner and Levitz, 2018). Dendritic SNARE fusion machinery has been implicated in the regulation of constitutive and activity-dependent glutamate receptor trafficking. Syntaxin-4 has previously been shown to regulate AMPAR trafficking in LTP, and surface expression of GluR2 and GluN1 in basal neurotransmission (Kennedy et al., 2010; Bin et al., 2018). Synaptosomal-associated proteins (SNAPs) are members of the plasma membrane-associated SNARE family required for glutamate receptor insertion. SNAP-25, heavily studied for its role in neurotransmitter release, has recently been shown to be involved in AMPAR insertion via formation of SNAP-25-syntaxin1A/B-VAMP2 complexes (Gu et al., 2016). SNAP-23, as a ubiquitously expressed SNAP-25 homolog, has been revealed to regulate NMDAR trafficking (Suh et al., 2010). Tomosyn was first identified as a syntaxin-1-binding protein that negatively regulated neurotransmitter release and exocytosis via interaction with SNAP-25 and syntaxin-1 (Hatsuzawa et al., 2003; Sakisaka et al., 2008), while later experiments in non-neuronal cells also showed that tomosyn regulates mast cell degranulation by switching interaction between syntaxin-4 and syntaxin-3 (Madera-Salcedo et al., 2018). This evidence suggests that tomosyn plays a role in glutamate receptor trafficking in hippocampal neurons via interaction with syntaxins and SNAPs. Our biochemical data showed that tomosyn indeed interacts with syntaxin-1, syntaxin-4, SNAP-25, and SNAP-23 in neuronal cells (Fig. 6 and 8). Knocking down tomosyn might conceivably have increased the surface insertion of glutamate

receptors through loss of inhibition of dendritic SNARE complex formation. However, we found instead that knockdown of tomosyn leads to decreased GluR1 surface expression (Fig. 8).

An increasing body of evidence shows that trafficking of AMPA receptors is actin-dependent (Hanley, 2014). For example, SNARE-mediated membrane fusion requires actin rearrangement (Porat-Shliom et al., 2013). Stable cytoskeletal structure is tightly modulated by de-polymerization and polymerization of actin, providing scaffolds to facilitate AMPAR trafficking along actin filaments (Allison et al., 1998; Kim and Lisman, 1999; Zhou et al., 2001). Although it has been shown that active glutamate receptors also regulate spine structural plasticity via modulation of RhoA activity (Schubert et al., 2006; Kang et al., 2009), our data suggest that the reduced surface expression of AMPA receptors is likely secondary to the increase of RhoA activity in tomosyn knockdown neurons. The increased RhoA activity in tomosyn knockdown neurons likely collapses the actin cytoskeleton, thereby disrupting the structure that supports AMPAR trafficking. Reduced GluR1 surface expression in tomosyn knockdown neurons coincided with reduced spine density and attenuated AMPAR-mediated mEPSC frequency. However, unchanged mEPSC amplitude suggests that the number of AMPA receptors in the remaining spines may be unchanged. Our C3T rescue experiments propose the dual functions for tomosyn in the regulation of neuronal stability and trafficking of glutamate receptors via the modulation of RhoA (Fig. 8G). Although the molecular mechanism is still unclear, it is plausible that tomosyn may function as a direct inhibitor of RhoA based on the characteristics described previously. Further investigation is required to address this question.

In the present study, the neuronal phenotypes of two tomosyn variants found in ASD were investigated to examine the potential contribution of L412V and Y502C mutations. ASD often features cellular characteristics involving altered dendritic structures and glutamate signaling

(Forrest et al., 2018; Moretto et al., 2018). Both L412V and Y502C mutants failed to completely restore total dendrite length following tomosyn knockdown, but only Y502C failed to rescue branch numbers from tomosyn knockdown cultures. L412V mutant also failed to rescue spine density, whereas Y502C partially restored the density of spines. FRET analysis confirmed that neither L412V nor Y502C mutant sufficiently suppressed increased RhoA activity in tomosyn knockdown neurons, which is consistent with the failure of the dendrite rescue phenotype. L412V and Y502C mutants also showed abnormal binding preference to dendritic SNARE proteins, including syntaxin-4 and SNAP-25. While both mutants strongly bound to syntaxin-4, L412V and Y502C showed opposite binding strengths with SNAP-25. The stronger interactions among L412V-Tom, syntaxin-4, and SNAP-25 likely inhibit functional dendritic SNARE formation, which coincides with the reduced surface expression of GluR1 and decreased spine density. Stronger interaction with syntaxin-4 but weaker binding with SNAP-25, however, may cause Y502C-Tom to produce inefficient inhibition of dendritic SNARE complexes and result in normal GluR1 surface expression and the rescue of spine density. Nevertheless, all these data suggest that L412V and Y502 mutations result in the loss-of-function of tomosyn and abrogate normal Rho signaling and trafficking of glutamate receptors. This mechanism may underlie the phenotype of disrupted neuronal structures often observed in ASD brains.

Taken together, this study uncovers a novel role of tomosyn in the maintenance of neuronal morphology and basal neuronal transmission via inhibition of RhoA activity. Our findings provide insight into tomosyn as a regulator for maintenance of neuronal stability and activity. It also broadens our understanding of how genetic variations in tomosyn may contribute to the etiology of ASD.

References

Allison DW, Gelfand VI, Spector I, Craig AM (1998) Role of actin in anchoring postsynaptic receptors in cultured hippocampal neurons: differential attachment of NMDA versus AMPA Receptors. J Neurosci 18:2423-2436 .

American Psychiatric Association (2013) Diagnostic and statistical manual of mental disorders, 5th Edn. : Arlington,VA: American Psychiatric Publishing: American Psychiatric Press, Inc.

Aoki K, Matsuda M (2009) Visualization of small GTPase activity with fluorescence resonance energy transfer-based biosensors. Nat Protoc 4:1623-1631.

Ashery U, Bielopolski N, Barak B, Yizhar O (2009) Friends and foes in synaptic transmission: the role of tomosyn in vesicle priming. Trends Neurosci 32:275-282.

Barak B, Williams A, Bielopolski N, Gottfried I, Okun E, Brown MA, Matti U, Rettig J, Stuenkel EL, Ashery U (2010) Tomosyn expression pattern in the mouse hippocampus suggests both presynaptic and postsynaptic functions. Front Neuroanat 4:149.

Barak B, Okun E, Ben-Simon Y, Lavi A, Shapira R, Madar R, Wang Y, Norman E, Sheinin A, Pita MA, Yizhar O, Mughal MR, Stuenkel E, van Praag H, Mattson MP, Ashery U (2013) Neuron-specific expression of tomosyn1 in the mouse hippocampal dentate gyrus impairs spatial learning and memory. Neuromolecular Med 15:351-363.

Batten SR, Matveeva EA, Whiteheart SW, Vanaman TC, Gerhardt GA, Slevin JT (2017) Linking kindling to increased glutamate release in the dentate gyrus of the hippocampus through the STXBP5/tomosyn-1 gene. Brain Behav 7:e00795.

Ben-Simon Y, Rodenas-Ruano A, Alviña K, Lam AD, Stuenkel EL, Castillo PE, Ashery U (2015) A combined optogenetic-knockdown strategy reveals a major role of tomosyn in mossy fiber synaptic plasticity. Cell Rep 12:396-404.

Bermejo MK, Milenkovic M, Salahpour A, Ramsey AJ (2014) Preparation of synaptic plasma membrane and postsynaptic density proteins using a discontinuous sucrose gradient. J Vis Exp:e51896.

Bin NR, Ma K, Harada H, Tien CW, Bergin F, Sugita K, Luyben TT, Narimatsu M, Jia Z, Wrana JL, Monnier PP, Zhang L, Okamoto K, Sugita S (2018) Crucial role of postsynaptic syntaxin 4 in mediating basal neurotransmission and synaptic plasticity in hippocampal CA1 neurons. Cell Rep 23:2955-2966.

Bridi MS, Park SM, Huang S (2017) Developmental disruption of GABA(A)R-Meditated inhibition in Cntnap2 KO mice. eNeuro 4:ENEURO.0162-0117.2017.

Cazares VA, Njus MM, Manly A, Saldate JJ, Subramani A, Ben-Simon Y, Sutton MA, Ashery U, Stuenkel EL (2016) Dynamic partitioning of synaptic vesicle pools by the SNARE-binding protein tomosyn. J Neurosci 36:11208-11222.

Chahrour M, O'Roak BJ, Santini E, Samaco RC, Kleiman RJ, Manzini MC (2016) Current perspectives in autism spectrum disorder: from genes to therapy. J Neurosci 36:11402-11410.

Cukier HN, Dueker ND, Slifer SH, Lee JM, Whitehead PL, Lalanne E, Leyva N, Konidari I, Gentry RC, Hulme WF, Booven DV, Mayo V, Hofmann NK, Schmidt MA, Martin ER, Haines JL, Cuccaro ML, Gilbert JR, Pericak-Vance MA (2014) Exome sequencing of extended families with autism reveals genes shared across neurodevelopmental and neuropsychiatric disorders. Mol Autism 5:1.

Davis LK, Meyer KJ, Rudd DS, Librant AL, Epping EA, Sheffield VC, Wassink TH (2009) Novel copy number variants in children with autism and additional developmental anomalies. J Neurodev Disord 1:292-301.

Diering GH, Huganir RL (2018) The AMPA receptor code of synaptic plasticity. Neuron 100:314-329.

Ferreira TA, Blackman AV, Oyrer J, Jayabal S, Chung AJ, Watt AJ, Sjostrom PJ, van Meyel DJ (2014) Neuronal morphometry directly from bitmap images. Nat Methods 11:982-984.

Forrest MP, Parnell E, Penzes P (2018) Dendritic structural plasticity and neuropsychiatric disease. Nat Rev Neurosci 19:215-234.

Fujita Y, Shirataki H, Sakisaka T, Asakura T, Ohya T, Kotani H, Yokoyama S, Nishioka H, Matsuura Y, Mizoguchi A, Scheller RH, Takai Y (1998) Tomosyn: a syntaxin-1-binding protein that forms a novel complex in the neurotransmitter release process. Neuron 20:905-915.

Govek EE, Newey SE, Akerman CJ, Cross JR, Van der Veken L, Van Aelst L (2004) The X-linked mental retardation protein oligophrenin-1 is required for dendritic spine morphogenesis. Nat Neurosci 7:364-372.

Groffen AJ, Jacobsen L, Schut D, Verhage M (2005) Two distinct genes drive expression of seven tomosyn isoforms in the mammalian brain, sharing a conserved structure with a unique variable domain. J Neurochem 92:554-568.

Gu Y, Chiu SL, Liu B, Wu PH, Delannoy M, Lin DT, Wirtz D, Huganir RL (2016) Differential vesicular sorting of AMPA and GABAA receptors. Proc Natl Acad Sci U S A 113:E922-931.

Hampson DR, Blatt GJ (2015) Autism spectrum disorders and neuropathology of the cerebellum. Front Neurosci 9:420-420.

Hanley JG (2014) Actin-dependent mechanisms in AMPA receptor trafficking. Front Cell Neurosci 8:381.

Hatsuzawa K, Lang T, Fasshauer D, Bruns D, Jahn R (2003) The R-SNARE motif of tomosyn forms SNARE core complexes with syntaxin 1 and SNAP-25 and down-regulates exocytosis. J Biol Chem 278:31159-31166.

Henley JM, Wilkinson KA (2016) Synaptic AMPA receptor composition in development, plasticity and disease. Nat Rev Neurosci 17:337-350.

Hussman JP, Chung R-H, Griswold AJ, Jaworski JM, Salyakina D, Ma D, Konidari I, Whitehead PL, Vance JM, Martin ER, Cuccaro ML, Gilbert JR, Haines JL, Pericak-Vance MA (2011) A noise-reduction GWAS analysis implicates altered regulation of neurite outgrowth and guidance in autism. Mol Autism 2:1.

Iossifov I et al. (2014) The contribution of de novo coding mutations to autism spectrum disorder. Nature 515:216-221.

Kagami M, Toh-e A, Matsui Y (1998) Sro7p, a Saccharomyces cerevisiae counterpart of the tumor suppressor l(2)gl protein, is related to myosins in function. Genetics 149:1717-1727.

Kang M-G, Guo Y, Huganir RL (2009) AMPA receptor and GEF-H1/Lfc complex regulates dendritic spine development through RhoA signaling cascade. Proc Natl Acad Sci U S A 106:3549-3554.

Kennedy MJ, Davison IG, Robinson CG, Ehlers MD (2010) Syntaxin-4 defines a domain for activity-dependent exocytosis in dendritic spines. Cell 141:524-535.

Kim C-H, Lisman JE (1999) A role of actin filament in synaptic transmission and long-term potentiation. J Neurosci 19:4314-4324.

Kopec CD, Li B, Wei W, Boehm J, Malinow R (2006) Glutamate receptor exocytosis and spine enlargement during chemically induced long-term potentiation. J Neurosci 26:2000-2009.

Lau CG, Zukin RS (2007) NMDA receptor trafficking in synaptic plasticity and neuropsychiatric disorders. Nat Rev Neurosci 8:413-426.

Lau CG, Takayasu Y, Rodenas-Ruano A, Paternain AV, Lerma J, Bennett MVL, Zukin RS (2010) SNAP-25 is a target of protein kinase C phosphorylation critical to NMDA receptor trafficking. J Neurosci 30:242-254.

Lehman K, Rossi G, Adamo JE, Brennwald P (1999) Yeast homologues of tomosyn and lethal giant larvae function in exocytosis and are associated with the plasma membrane SNARE, Sec9. J Cell Biol 146:125-140.

Li J, Zhang W, Yang H, Howrigan DP, Wilkinson B, Souaiaia T, Evgrafov OV, Genovese G, Clementel VA, Tudor JC, Abel T, Knowles JA, Neale BM, Wang K, Sun F, Coba MP (2017) Spatiotemporal profile of postsynaptic interactomes integrates components of complex brain disorders. Nat Neurosci 20:1150-1161.

Lin YC, Koleske AJ (2010) Mechanisms of synapse and dendrite maintenance and their disruption in psychiatric and neurodegenerative disorders. Annu Rev Neurosci 33:349-378.

Lin YC, Yeckel MF, Koleske AJ (2013) Abl2/Arg controls dendritic spine and dendrite arbor stability via distinct cytoskeletal control pathways. J Neurosci 33:1846-1857.

Lin YC, Frei JA, Kilander MB, Shen W, Blatt GJ (2016) A subset of autism-associated genes regulate the structural stability of neurons. Front Cell Neurosci 10:263.

Madera-Salcedo IK, Danelli L, Tiwari N, Dema B, Pacreau E, Vibhushan S, Birnbaum J, Agabriel C, Liabeuf V, Klingebiel C, Menasche G, Macias-Silva M, Benhamou M, Charles N, González-Espinosa C, Vitte J, Blank U (2018) Tomosyn functions as a PKCδ-regulated fusion clamp in mast cell degranulation. Sci Signal 11.

Masuda ES, Huang BC, Fisher JM, Luo Y, Scheller RH (1998) Tomosyn binds t-SNARE proteins via a VAMP-like coiled coil. Neuron 21:479-480.

Matsuda T, Cepko CL (2004) Electroporation and RNA interference in the rodent retina in vivo and in vitro. Proc Natl Acad Sci U S A 101:16-22.

Matsunami N, Hadley D, Hensel CH, Christensen GB, Kim C, Frackelton E, Thomas K, da Silva RP, Stevens J, Baird L, Otterud B, Ho K, Varvil T, Leppert T, Lambert CG, Leppert M, Hakonarson H (2013) Identification of rare recurrent copy number variants in high-risk autism families and their prevalence in a large ASD population. PloS One 8:e52239.

Mechler BM, McGinnis W, Gehring WJ (1985) Molecular cloning of lethal(2)giant larvae, a recessive oncogene of Drosophila melanogaster. The EMBO J 4:1551-1557.

Meijering E, Jacob M, Sarria JC, Steiner P, Hirling H, Unser M (2004) Design and validation of a tool for neurite tracing and analysis in fluorescence microscopy images. Cytometry 58 A:167-176.

Moretto E, Murru L, Martano G, Sassone J, Passafaro M (2018) Glutamatergic synapses in neurodevelopmental disorders. Prog Neuro-Psychopharmacol Biol Psychiatry 84:328-342.

Nakayama AY, Harms MB, Luo L (2000) Small GTPases Rac and Rho in the maintenance of dendritic spines and branches in hippocampal pyramidal neurons. J Neurosci 20:5329-5338.

Noel J, Ralph GS, Pickard L, Williams J, Molnar E, Uney JB, Collingridge GL, Henley JM (1999) Surface expression of AMPA receptors in hippocampal neurons is regulated by an NSF-dependent mechanism. Neuron 23:365-376.

Oblak AL, Gibbs TT, Blatt GJ (2010) Decreased GABA(B) receptors in the cingulate cortex and fusiform gyrus in autism. J Neurochem 114:1414-1423.

Oblak AL, Gibbs TT, Blatt GJ (2011) Reduced GABAA receptors and benzodiazepine binding sites in the posterior cingulate cortex and fusiform gyrus in autism. Brain Res 1380:218-228.

Pertz O, Hodgson L, Klemke RL, Hahn KM (2006) Spatiotemporal dynamics of RhoA activity in migrating cells. Nature 440:1069-1072.

Porat-Shliom N, Milberg O, Masedunskas A, Weigert R (2013) Multiple roles for the actin cytoskeleton during regulated exocytosis. Cell Mol Life Sci 70:2099-2121.

Reiner A, Levitz J (2018) Glutamatergic signaling in the central nervous system: ionotropic and metabotropic receptors in concert. Neuron 98:1080-1098.

Rossi G, Watson K, Kennedy W, Brennwald P (2018) The tomosyn homologue, Sro7, is a direct effector of the Rab GTPase, Sec4, in post-Golgi vesicle tethering. Mol Biol Cell 29:1476-1486.

Rossi G, Watson K, Demonch M, Temple B, Brennwald P (2015) In vitro reconstitution of Rab GTPase-dependent vesicle clustering by the yeast lethal giant larvae/tomosyn homolog, Sro7. J Biol Chem 290:612-624.

Sakisaka T, Baba T, Tanaka S, Izumi G, Yasumi M, Takai Y (2004) Regulation of SNAREs by tomosyn and ROCK: implication in extension and retraction of neurites. J Cell Biol 166:17-25.

Sakisaka T, Yamamoto Y, Mochida S, Nakamura M, Nishikawa K, Ishizaki H, Okamoto-Tanaka M, Miyoshi J, Fujiyoshi Y, Manabe T, Takai Y (2008) Dual inhibition of SNARE complex formation by tomosyn ensures controlled neurotransmitter release. J Cell Biol 183:323-337.

Saldate JJ, Shiau J, Cazares VA, Stuenkel EL (2018) The ubiquitin-proteasome system functionally links neuronal tomosyn-1 to dendritic morphology. J Biol Chem 293:2232-2246.

Sanders SJ et al. (2015) Insights into autism spectrum disorder genomic architecture and biology from 71 risk loci. Neuron 87:1215-1233.

Schapira M, Tyers M, Torrent M, Arrowsmith CH (2017) WD40 repeat domain proteins: a novel target class? Nat Rev Drug Discov 16:773-786.

Schubert V, Da Silva JS, Dotti CG (2006) Localized recruitment and activation of RhoA underlies dendritic spine morphology in a glutamate receptor-dependent manner. J Cell Biol 172:453-467.

Short PJ, McRae JF, Gallone G, Sifrim A, Won H, Geschwind DH, Wright CF, Firth HV, FitzPatrick DR, Barrett JC, Hurles ME (2018) De novo mutations in regulatory elements in neurodevelopmental disorders. Nature 555:611-616.

Subauste MC, Von Herrath M, Benard V, Chamberlain CE, Chuang TH, Chu K, Bokoch GM, Hahn KM (2000) Rho family proteins modulate rapid apoptosis induced by cytotoxic T lymphocytes and Fas. J Biol Chem 275:9725-9733.

Subramanian K, Brandenburg C, Orsati F, Soghomonian J-J, Hussman JP, Blatt GJ (2017) Basal ganglia and autism – a translational perspective. Autism Res 10:1751-1775.

Suh YH, Terashima A, Petralia RS, Wenthold RJ, Isaac JT, Roche KW, Roche PA (2010) A neuronal role for SNAP-23 in postsynaptic glutamate receptor trafficking. Nat Neurosci 13:338-343.

Volk L, Chiu SL, Sharma K, Huganir RL (2015) Glutamate synapses in human cognitive disorders. Annu Rev Neurosci 38:127-149.

Widberg CH, Bryant NJ, Girotti M, Rea S, James DE (2003) Tomosyn interacts with the t-SNAREs syntaxin4 and SNAP23 and plays a role in insulin-stimulated GLUT4 translocation. J Biol Chem 278:35093-35101.

Ye S, Huang Y, Joshi S, Zhang J, Yang F, Zhang G, Smyth SS, Li Z, Takai Y, Whiteheart SW (2014) Platelet secretion and hemostasis require syntaxin-binding protein STXBP5. J Clin Invest 124:4517-4528.

Zhou Q, Xiao M, Nicoll RA (2001) Contribution of cytoskeleton to the internalization of AMPA receptors. Proc Natl Acad Sci U S A 98:1261-1266.

Zhu Q, Yamakuchi M, Ture S, de la Luz Garcia-Hernandez M, Ko KA, Modjeski KL, LoMonaco MB, Johnson AD, O'Donnell CJ, Takai Y, Morrell CN, Lowenstein CJ (2014) Syntaxin-binding protein STXBP5 inhibits endothelial exocytosis and promotes platelet secretion. J Clin Invest 124:4503-4516.

Figure Legends

Figure 1. Tomosyn is localized in both pre- and post-synaptic compartments. ***A***, Western blot analysis shows the developmental expression pattern of tomosyn protein in mouse whole brain at P0, P7, P14, and P21. ***B***, Spatial expression of tomosyn in different brain regions at P14. CX, cortex; HC, hippocampus; Th/St, thalamus and striatum; CB, cerebellum. ***C***, Temporal expression pattern of tomosyn in the hippocampus at P0, P7, P14, and P21. ***D***, Temporal expression of tomosyn and PSD-95 in cultured cortical neurons at 1, 4, 7, 10, and 14 DIV. ***E***, Confocal immunofluorescent images showing tomosyn (green), MAP2 (red), and DAPI (blue) from a cultured hippocampal neuron at 15 DIV. Scale bar, 50 μm. ***F***, Confocal images of a dendritic spine of a cultured neuron transfected with RFP and tomosyn-GFP. ***G***, Fluorescence intensity of tomosyn-GFP and RFP in the dendritic spine versus the dendritic shaft was quantified by line scan (shown in ***F***). ***H***, Synaptic fractionation of forebrain lysates (total) shows the subcellular localization of tomosyn in P21 mouse brains. P1, nuclei; S1,cytosol/membranes; P2, crude synaptosomes; S2, cytosol/light membranes; P3, synaptosomes; SPM, synaptic plasma membranes; PSD, post-synaptic density; S3, synaptic vesicles. ***I***, Fluorescent images showing either CaMKIIα or GAD67 and tomosyn form cultured hippocampal neurons at 15 DIV. Scale bar, 20 μm. Three independent experiments in ***A***-***D*** and ***H***, 29 spines in ***G***.

Figure 2. Knockdown of tomosyn reduces dendritic complexity and dendritic spine density.

A, Western blot analysis shows the knockdown efficiency of shRNAs against tomosyn. Tomosyn-GFP was co-transfected with scrambled shRNA, shRNA482, or shRNA1083 in N2a cells. shRNA482 resulted in the most effective reduction of tomosyn protein level and was

shown as shTomosyn in subsequent experiments. ****$p < 0.0001$ compared to scramble control. One-way ANOVA with Dunnett's multiple-comparison tests; three independent experiments. ***B***, Western blot analysis shows the protein level of Tom^r-GFP, a shRNA-resistant form of tomosyn, in tomosyn-knockdown N2a cells. While shTomosyn reduced the expression of Tom-GFP, the protein level of Tom^r-GFP was not affected by shTomosyn knockdown. **$p < 0.01$ when compared with shTomosyn + Tom-GFP. One-way ANOVA with Dunnett's multiple-comparison tests; three independent experiments. ***C***, Representative images of reconstructed dendritic tress from mouse hippocampal neurons transfected with scrambled shRNA + GFP or shTomosyn + GFP or shTomosyn + Tom^r-GFP. Scale bar, 100 μm. ***D***, Sholl analysis of reconstructed neurons. Neurons expressing shTomosyn exhibited compromised dendritic complexity, whereas expression of Tom^r-GFP rescued simplified dendritic complexity in shTomosyn-expressing neurons compared to scramble control. * indicates significant difference at a particular radius compared to scramble control, Two-way ANOVA with Tukey's test, n = 23~25 neurons from three different cultures. ***E***, Confocal fluorochrome images of dendritic spines from neurons transfected with scrambled shRNA + GFP, shTomosyn + GFP, or shTomosyn + Tom^r-GFP for 72 hrs. Scale bar, 2 μm. ***F***, Mean spine density was decreased in tomosyn knockdown neurons, whereas spine density was restored in Tom^r-GFP and shTomosyn-co-expressing neurons compared to shTomosyn + GFP. ****$p < 0.0001$. One-way ANOVA with Dunnett's multiple-comparison tests. n = 29~31 neurons from three different cultures.

Figure 3. Frequency of miniature EPSCs is decreased in tomosyn knockdown neurons. Cultured hippocampal neurons were transfected with either scrambled shRNA or shTomosyn. ***A,*** An example of current traces collected from whole-cell voltage-clamp of hippocampal neurons.

B, Examples of average (top) and scaled (bottom) mEPSC traces from shTomosyn and control neurons. Summary graphs show ***C,*** frequency (****$p < 0.0001$) ***D***, amplitude ($p = 0.32$), and ***E***, charge (*$p < 0.05$) of recorded mEPSCs. Summary graph showing kinetic properties of mEPSCs, including ***F,*** decay time constant (*$p < 0.05$). ***C*** by Mann-Whitney test; ***D, E, F*** by unpaired student's *t* test with Welch's correction. n = 22 neurons for scramble, n = 21 neurons for shTomosyn from five independent cultures.

Figure 4. Tomosyn knockdown results in increased RhoA activity in hippocampal neurons. Hippocampal neurons were co-transfected with a RhoA Biosensor and either scrambled shRNA or shTomosyn. ***A***, Representative images show the neurons in the intensity-modulated display mode. Scale bar, 10 μm. ***B***, FRET efficiency was determined as a ratio of YFP/CFP. n = 69 ~ 72 neurons per condition, four independent experiments, two-tailed Mann-Whitney test, *$p < 0.05$. ***C***, pbFRET was used to measure RhoA activity in different dendritic areas. Representative images of dendritic segments taken immediately before and after photobleaching. Bleached area was highlighted as a white dashed circle (ROI). Scale bar, 2 μm. ***C'***, A representative graph of pbFRET experiment shows changes in fluorescence intensities within bleach ROI over the course of 10 frames. Photobleaching was performed after the 5th frame. ***D***, FRET efficiency was determined by calculating percentage (%) of increase in donor fluorescence intensity after acceptor photobleaching. Tomosyn knockdown neuron showed higher FRET ratio. ****$p <$ 0.0001 when compared to scramble control. No significant FRET efficiency percentage (%) of increase was found between apical dendrites and basal dendrites within each group. $F_{(1, 57)} =$ 0.0093, $p = 0.9234$. n = 17 neurons per condition, four independent experiments. Factor: dendrite region. Two-way ANOVA with Tukey's test. ***E***, Schematic structure of domain mutant tomosyn.

FL-Tom, full-length mouse tomosyn (1-1166 aa); Tom-ΔC, containing a N-terminal domain with WD40 repeats (1-1048 aa); Tom-ΔN, containing a SNARE coil-coiled domain (1049-1099 aa). ***F***, Western blot shows expression of domain mutant tomosyn (Tom-ΔC-RFP and Tom-ΔN-RFP), FL-Tom-RFP and RFP control in N2a cells. ***G***, Representative graph showing FRET efficiency in domain mutant tomosyn-expressing neuron. Neurons with Tom-ΔN-RFP showed increased FRET efficiency. ****$p < 0.0001$ compared to RFP vector. n = 28 ~ 32 neurons per condition, four independent experiments. One-way ANOVA with Dunnett's multiple-comparison tests.

Figure 5. Inhibition of the Rho signaling pathway restores altered dendritic structures in tomosyn knockdown neurons.

A, Total dendrite length, ***B***, branch number, and ***C***, spine density of neurons co-transfected with T19N-RhoA exhibited similar levels between scramble control and shTomosyn-expressing neurons. Tomosyn knockdown neurons treated with C3T, but not Y27632, rescued the ***D,*** total dendrite length, ***E***, branch number, and ***F***, spine density. *$p < 0.05$, **$p < 0.01$, ***$p < 0.001$, ****$p < 0.0001$, Two-way ANOVA with Sidak's multiple comparisons test. n = 27 ~ 35 neurons per condition in ***A*** and ***B***; n = 18 ~ 26 neurons per condition in ***C***; n = 23~32 neurons per condition in ***D*** and ***E***; n = 23 ~ 30 neurons per condition in ***F***.

Figure 6: Surface-expression of GluR1 subunits is reduced in tomosyn knockdown neurons. ***A***, Western blot analysis of co-immunoprecipitation experiments in cultured cortical neurons. Cultured cortical neuron lysates at 15 DIV were immunoprecipitated with either anti-

tomosyn antibody, rabbit IgG isotype control, anti-syntaxin-4 antibody, or mouse IgG isotype control. Immunoblot was probed with anti-tomosyn and anti-syntaxin-4 antibodies. W = wash. ***B***, Representative Western blot and densitometry graph show the expression of tomosyn and syntaxin-4 in N2a cells transfected with scrambled shRNA and shTomosyn. Two-way ANOVA with Tukey's multiple-comparison tests, ****$p < 0.0001$, five independent cultures. ***C***, Representative confocal images showing the surface staining of the GluR1 subunit of AMPA receptors in cultured hippocampal neurons at 15 DIV. Neurons were co-transfected with scrambled shRNA or shTomosyn and pHluorin-GluR1. Tomosyn knockdown neurons were treated with the RhoA inhibitor, C3T. Scale bar, 2µm. ***D***, Quantification of surface expression of pHluorin-GluR1 was shown on the right. *$p < 0.05$. One-way ANOVA with Dunnett's multiple-comparison tests; n = 20 ~ 25 neurons per condition; three independent experiments.

Figure 7: Autism-associated mutant tomosyn fails to restore dendritic arborization and spine loss in tomosyn knockdown neurons. ***A***, An illustration of the location of L412V and Y502C mutations in tomosyn. ***B***, Representative Western blot and densitometry graph show protein level of shRNA resistant WT^r-Tom-GFP, L412V^r-Tom-GFP, and Y502C^r-Tom-GFP in N2a cells co-transfected with shTomosyn. **$p < 0.01$, *** $p < 0.001$, One-way ANOVA with Dunnett's multiple-comparison tests; three independent experiments. ***C***, Representative graph showing FRET efficiency in tomosyn knockdown neurons rescued with WT^r, L412V^r, or Y502C^r tomosyn constructs. Neurons were co-transfected with a FRET biosensor and scrambled shRNA, shTomosyn, shTomosyn-WT^r-Tom-RFP, shTomosyn-L412V^r-Tom-RFP, or shTomosyn-Y502C^r-Tom-RFP. *$p < 0.05$, ***$p < 0.001$. Four independent experiments. One-way ANOVA with Dunnett's multiple-comparison tests. ***D***, Representative images of reconstructed dendritic

trees, ***E***, total length, and ***F***, branch number from mouse hippocampal neurons transfected with scrambled shRNA + GFP, shTomosyn + GFP, shTomosyn + WT^r-Tom-GFP, shTomosyn +L412V^r-Tom-GFP, or shTomosyn + Y502C^r-Tom-GFP. Scale bar, 100 µm. Both L412V and Y502C mutant tomosyn failed to rescue total dendrite length compared to scrambled shRNA. Only Y502C failed to rescue branch number compared to scrambled shRNA (*$p < 0.05$, ***$p < 0.001$, ****$p < 0.0001$). One-way ANOVA with Dunnett's multiple-comparison tests; n = 26 ~ 34 neurons per condition; three independent experiments. ***G***, Representative confocal images show morphology of dendritic spines in cultured hippocampal neurons transfected with different tomosyn constructs. Neurons were co-transfected with scrambled shRNA and GFP, shTomosyn and GFP, shTomosyn together with WT^r-Tom-GFP, shTomosyn together with L412V^r-Tom-GFP, or shTomosyn together with Y502C^r-Tom-GFP. Scale bar, 2 µm. ***H***, quantification of spine density. ****$p < 0.0001$. One-way ANOVA with Dunnett's multiple-comparison tests; n = 29 ~ 31 neurons per condition; three independent experiments.

Figure 8: Surface expression of GluR1 is decreased in neurons expressing autism-associated tomosyn variants. Western blot analysis of co-immunoprecipitation experiments in N2a cells. Normalized quantifications are on the right. Cells were either untransfected (UT) or transfected with c-Myc-tagged WT-Tom, L412V-Tom, or Y512C-Tom. Protein extracts were immunoprecipitated by anti-c-Myc-antibody-coupled beads and immunoblotted with anti-c-Myc, anti-syntaxin-1, anti-syntaxin-4, anti-SNAP-23, and anti-SNAP-25 antibodies. ***A***, No significant difference of binding to syntaxin-1 with either L412V-Tom or Y502C-Tom was found compared to WT-Tom (*p* = 0.9965). ***B***, Both L412V- and Y502C-Tom bound stronger to syntaxin-4 compared to WT (*$p < 0.05$). ***C***, L412V-Tom bound stronger to SNAP-25, whereas Y502C-Tom

bound more weakly compared to WT-Tom (*$p < 0.05$). ***D***, No significant difference of binding to SNAP-23 with either L412V or Y502C was detected compared to WT-Tom ($p = 0.37$). One-way ANOVA with Dunnett's multiple-comparison tests; three independent experiments. ***E***, Example confocal images show the surface expression of GluR1 in neurons expressing shTomosyn-WT^r-Tom-RFP, shTomosyn-L412V^r-Tom-RFP or shTomosyn-Y502C^r-Tom-RFP together with pHluorin-GluR1. ***F,*** A reduction of GluR1 surface expression in neurons co-expressing shTomosyn-L412V^r-Tom-RFP, compared to shTomosyn-WT^r-Tom-RFP, was observed. (**$p <$ 0.01, ***$p < 0.001$), One-way ANOVA with Dunnett's multiple-comparison tests; n =17~ 23 neurons per condition three independent experiments. ***G***, Schematic model of spine loss and GluR1 trafficking impairment in tomosyn knockdown or mutant neurons (left). Tomosyn has dual roles in the maintenance of dendritic stability and AMPA receptor trafficking (right). Tomosyn regulates dendritic stability and AMPA receptor trafficking via inhibition of the RhoA signaling pathway, and mutations in tomosyn likely affect AMPA receptors via differential binding with dendritic SNARE proteins, including syntaxin-4, and SNAP-25, and lack of RhoA inhibition.

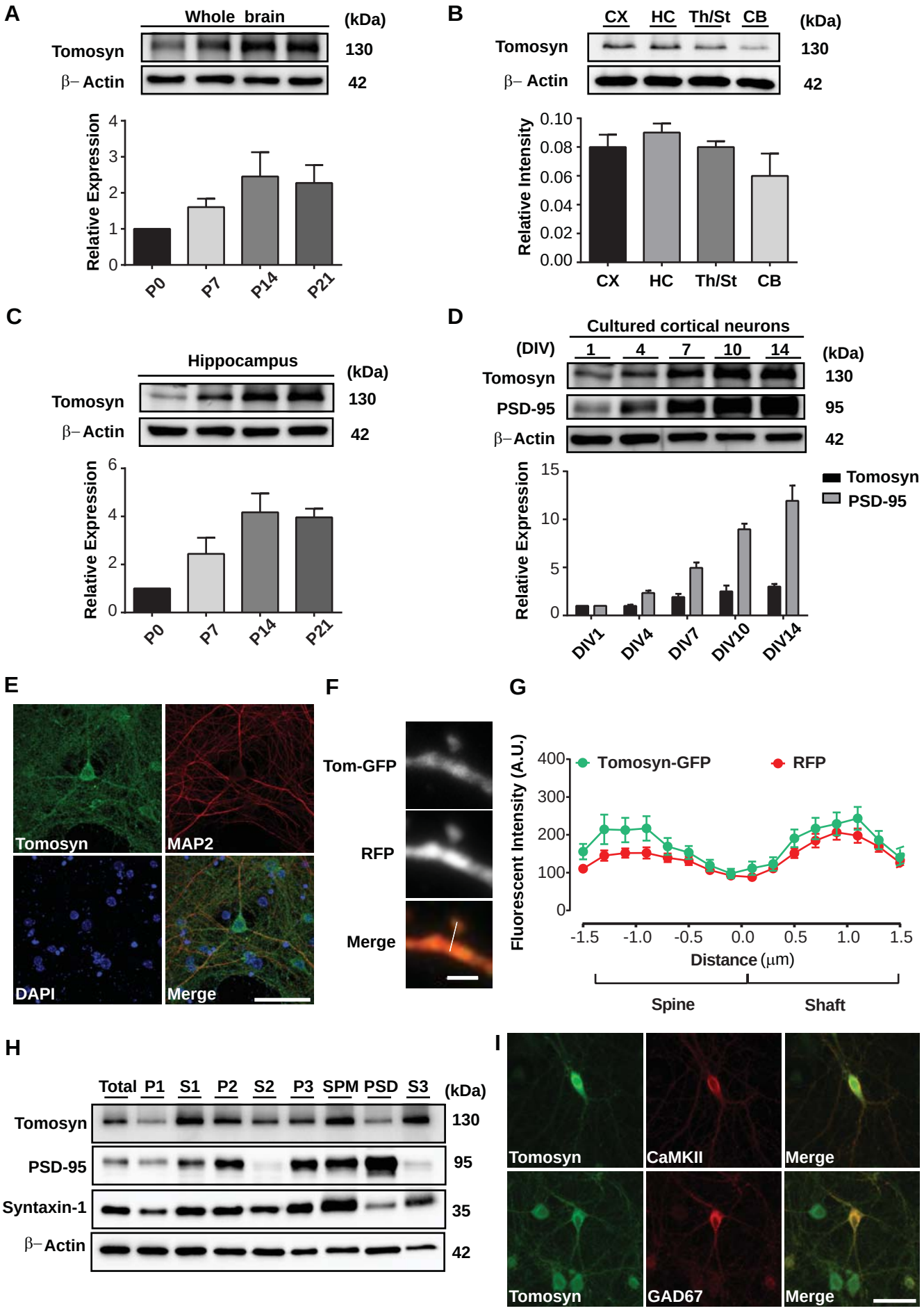

Figure 1. Shen et al., 2019

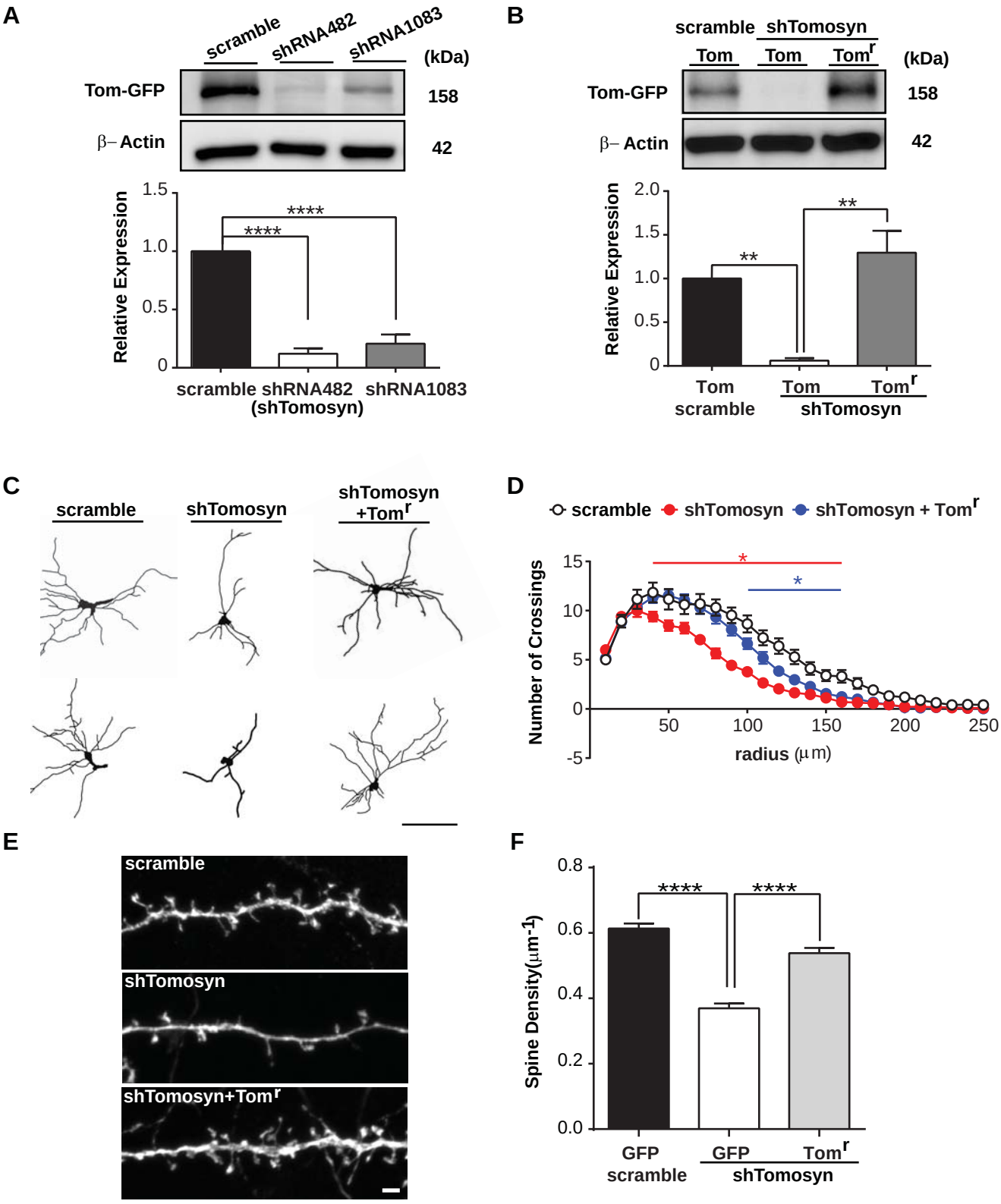

Figure 2. Shen et al., 2019

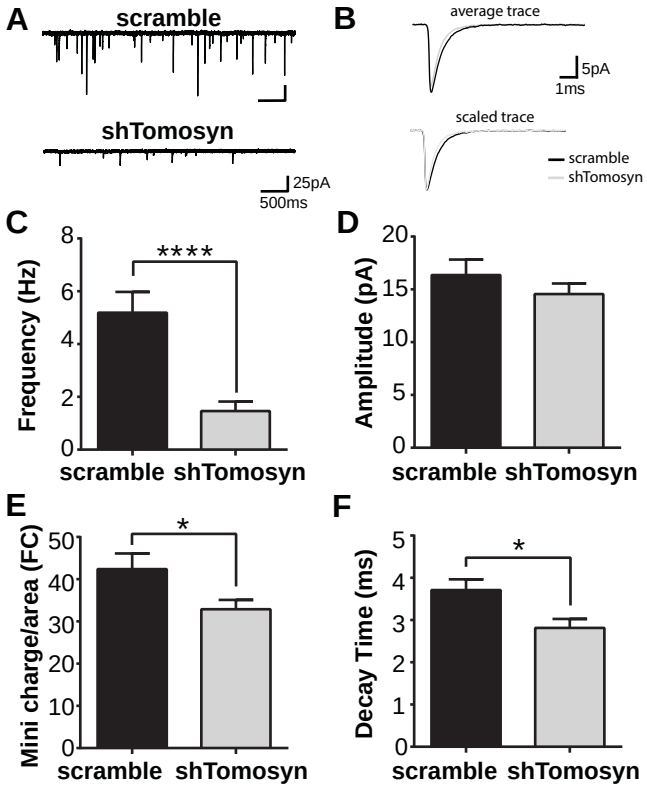

Figure 3. Shen et al., 2019

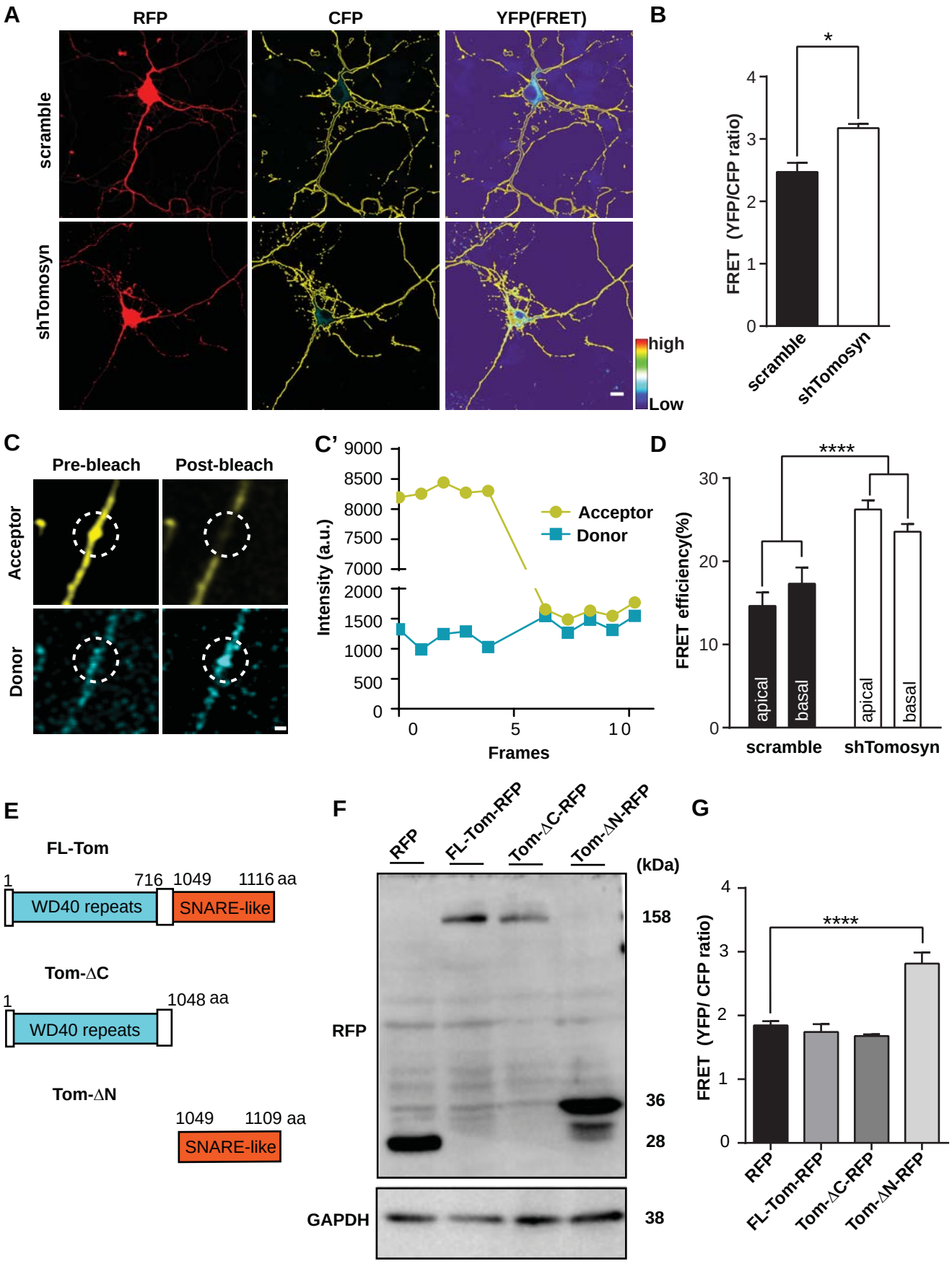

Figure 4. Shen et al., 2019

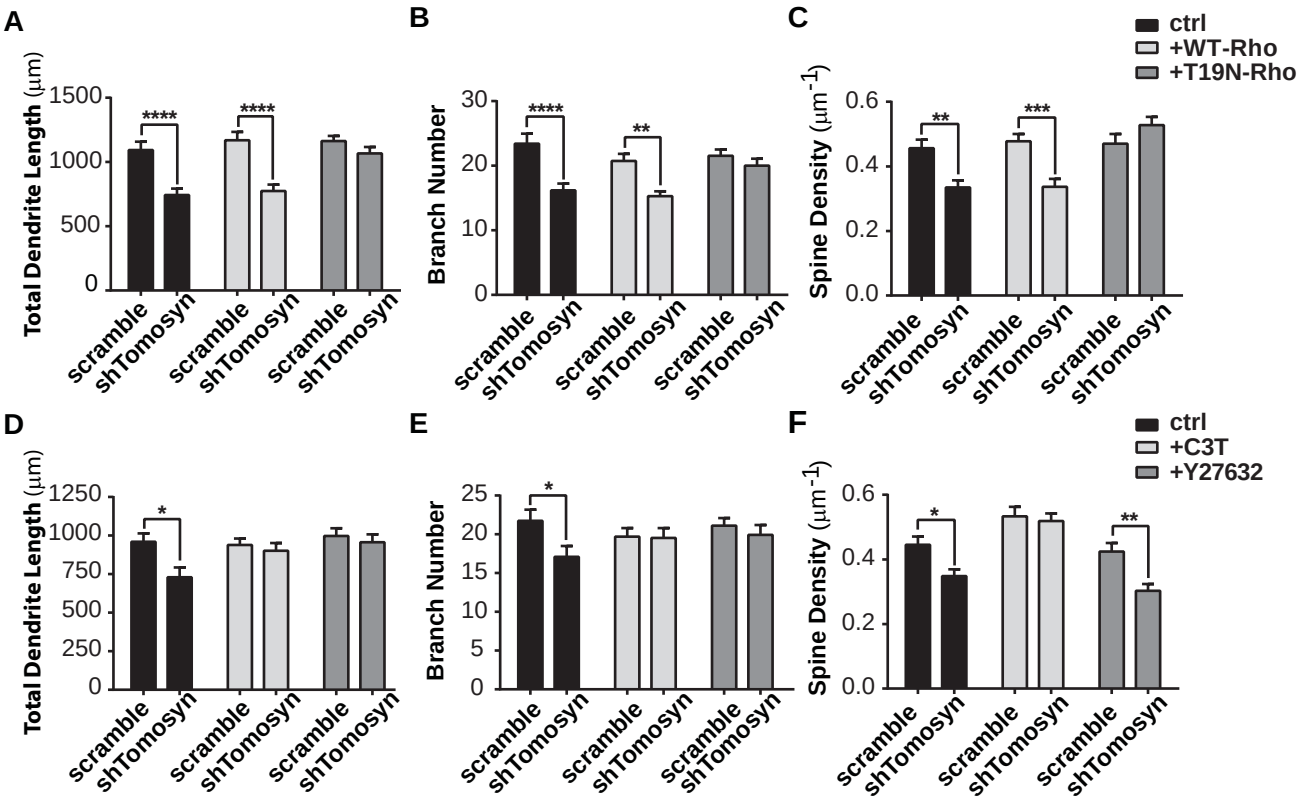

Figure 5. Shen et al., 2019

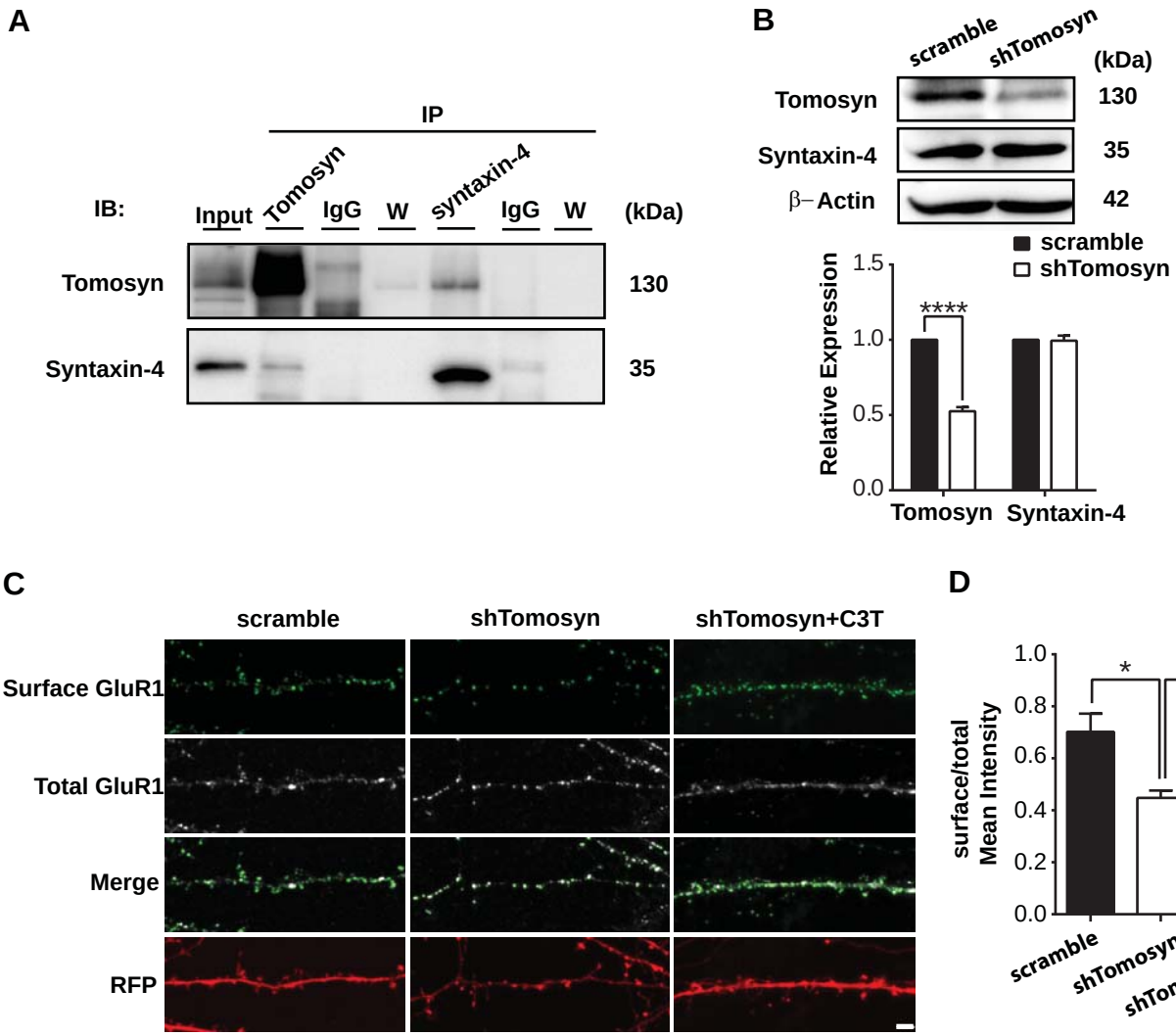

Figure 6. Shen et al., 2019

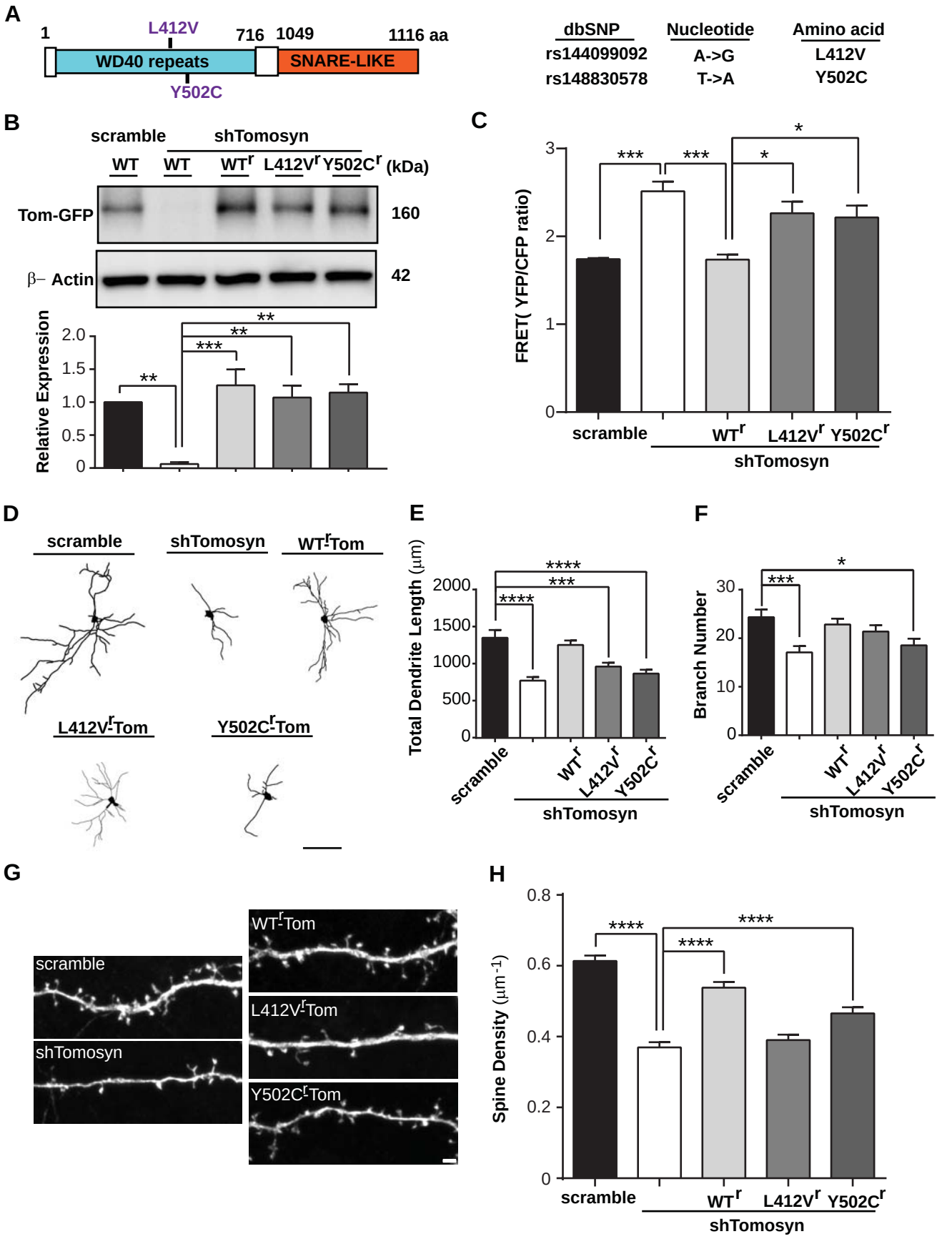

Figure 7. Shen et al.,2019

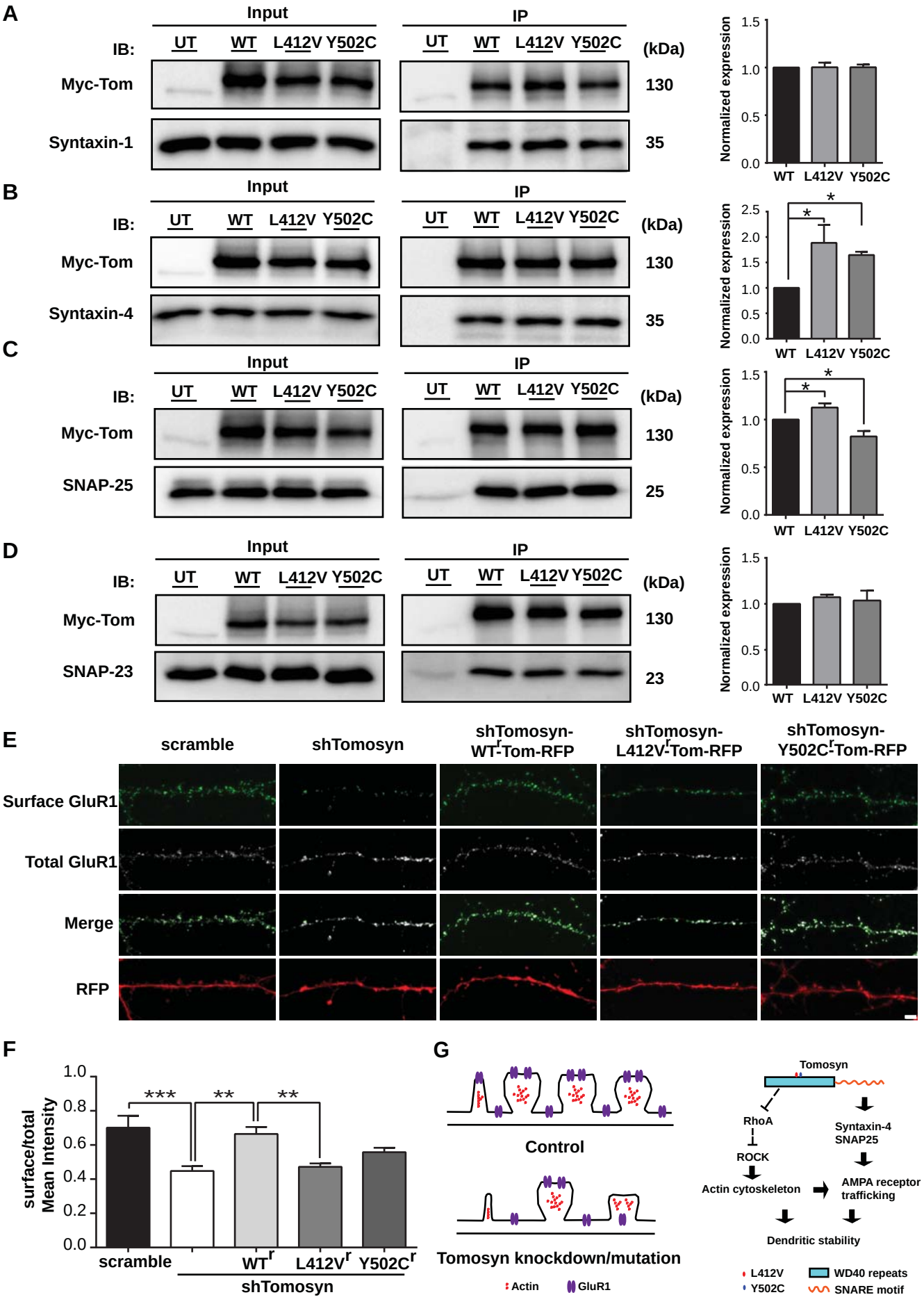

Figure 8. Shen et al., 2019